

# Methodology for Formulating Diesel Surrogate Fuels with Accurate Compositional, Ignition-Quality, and Volatility Characteristics

Charles J. Mueller,<sup>\*,†</sup> William J. Cannella,<sup>‡</sup> Thomas J. Bruno,<sup>§</sup> Bruce Bunting,<sup>||</sup> Heather D. Dettman,<sup>⊥</sup> James A. Franz,<sup>#,§</sup> Marcia L. Huber,<sup>§</sup> Mani Natarajan,<sup>▽</sup> William J. Pitz,<sup>○</sup> Matthew A. Ratcliff,<sup>◆</sup> and Ken Wright<sup>¶</sup>

<sup>†</sup>Sandia National Laboratories, East Avenue, Livermore, California 94550

<sup>‡</sup>Chevron Corporation, Chevron Way, Richmond, California 94802

<sup>§</sup>National Institute of Standards and Technology, Boulder, Colorado 80305

<sup>||</sup>Oak Ridge National Laboratory, Bethel Valley Road, Oak Ridge, Tennessee 37831

<sup>⊥</sup>Natural Resources Canada (CanmetENERGY), Devon, Alberta T9G 1A6, Canada

<sup>#</sup>Pacific Northwest National Laboratory, Battelle Boulevard, Richland, Washington, 99352

<sup>▽</sup>Marathon Petroleum Company, Main Street, Findlay, Ohio, 45840

<sup>○</sup>Lawrence Livermore National Laboratory, East Avenue, Livermore, California 94550

<sup>◆</sup>National Renewable Energy Laboratory, Golden, Colorado 80401

<sup>¶</sup>Phillips 66 Company, Bartlesville, Oklahoma 74003

**ABSTRACT:** In this study, a novel approach was developed to formulate surrogate fuels having characteristics that are representative of diesel fuels produced from real-world refinery streams. Because diesel fuels typically consist of hundreds of compounds, it is difficult to conclusively determine the effects of fuel composition on combustion properties. Surrogate fuels, being simpler representations of these practical fuels, are of interest because they can provide a better understanding of fundamental fuel-composition and property effects on combustion and emissions-formation processes in internal-combustion engines. In addition, the application of surrogate fuels in numerical simulations with accurate vaporization, mixing, and combustion models could revolutionize future engine designs by enabling computational optimization for evolving real fuels. Dependable computational design would not only improve engine function, it would do so at significant cost savings relative to current optimization strategies that rely on physical testing of hardware prototypes. The approach in this study utilized the state-of-the-art techniques of <sup>13</sup>C and <sup>1</sup>H nuclear magnetic resonance spectroscopy and the advanced distillation curve to characterize fuel composition and volatility, respectively. The ignition quality was quantified by the derived cetane number. Two well-characterized, ultra-low-sulfur #2 diesel reference fuels produced from refinery streams were used as target fuels: a 2007 emissions certification fuel and a Coordinating Research Council (CRC) Fuels for Advanced Combustion Engines (FACE) diesel fuel. A surrogate was created for each target fuel by blending eight pure compounds. The known carbon bond types within the pure compounds, as well as models for the ignition qualities and volatilities of their mixtures, were used in a multiproperty regression algorithm to determine optimal surrogate formulations. The predicted and measured surrogate-fuel properties were quantitatively compared to the measured target-fuel properties, and good agreement was found.

## 1. INTRODUCTION

Reciprocating internal-combustion engines and their fuels are evolving rapidly to address concerns about energy security and environmental quality. There is particular interest in compression-ignition (CI or diesel-cycle) engines because they have inherently higher efficiencies than spark-ignition engines. Furthermore, CI engines can burn a wide range of fuels (including renewable and unconventional fuels) using low-emission, advanced-combustion strategies that are currently under development.<sup>1–9</sup>

It is challenging to make strategic engine and fuel design changes when the engine technology, fuel composition, and combustion strategy are all simultaneously changing. The parameter space is too large to be optimized using a traditional build-and-test methodology. As a result, new computational

tools and surrogate fuels are required to facilitate the design and optimization of emerging fuels for advanced engines in the most cost- and time-efficient manner.<sup>10,11</sup>

In addition to being useful for computational studies, surrogate fuels are important for experimental work. Their simpler compositions can facilitate insights into fuel-composition and property effects on the in-cylinder vaporization, mixing, and combustion processes that ultimately determine engine efficiency, emissions, performance, and aftertreatment-system requirements.<sup>6,12–16</sup> Surrogate fuels also have value as time-invariant reference fuels for experimental studies. The

Received: February 20, 2012

Revised: May 8, 2012

Published: May 22, 2012



compositions of real diesel fuels (even reference diesel fuels) vary over time because the compositions of the individual refinery streams that are blended to make finished fuels vary with the type of crude oil and/or other feedstocks being processed, refinery processing strategies, regulations on fuel composition or other properties, and liquid-phase reactions that occur during long-term storage. Hence, surrogate fuels have value as standards that can be used to evaluate different engine-combustion strategies at different times without the usual confounding effects of fuel-composition changes.

There has been much previous work on characterizing diesel surrogate components and their mixtures. These efforts were reviewed by Pitz and Mueller.<sup>12</sup> Most of the previously studied surrogate mixtures contained a small number of components (up to six) and focused on matching the ignition, oxidation, flame extinction, and sooting levels of the target diesel fuel.<sup>17–20</sup> Only a few studies have tried to match the vaporization characteristics of real diesel fuel with the surrogate. Based on their computational modeling, Ra and Reitz<sup>21</sup> found that it was important to match the distillation curve of the diesel fuel because the light components tend to preferentially vaporize upstream in the diesel spray and the heavier components downstream. Dooley et al.<sup>22</sup> described a systematic way to match a surrogate jet fuel to the real target fuel by matching the derived cetane number (DCN), H/C ratio, average molecular weight, and threshold sooting index<sup>23</sup> of the target fuel with the surrogate. Liang et al.<sup>16</sup> created a four-component diesel surrogate that matched the cetane number, C/H ratio by weight, lower heating value, and 50 vol % distillation temperature of a U.S. #2 diesel fuel using surrogate blend optimizer<sup>24</sup> software.

The present study provides a methodology for creating surrogate diesel fuels with improved fidelity in matching the molecular structures, ignition quality, and distillation characteristics of their target diesel fuels. This study also provides an alternative systematic and automated way of matching selected properties of the surrogate with those of the target fuel by employing a regression model. These are key steps toward the realization of surrogate diesel fuels that match the vaporization, ignition, combustion, and emissions behaviors of their target fuels with acceptable accuracy. Given the rapid pace of advancements in computational capabilities, it was decided to create eight-component surrogates from compounds that are more representative of those found in market diesel fuels, to create surrogates that will be useful regardless of the application. This strategy was selected with the understanding that the resulting detailed kinetic mechanisms can be reduced more aggressively when circumstances allow.

**1.1. Approach.** It is useful to define the key terms used in this paper related to the formulation of surrogate fuels; this is done in Figure 1. The concepts of a *target fuel* and a *surrogate fuel* should be clear from the figure and the preceding discussion. A *surrogate design property* is a characteristic of the target fuel that is to be matched by the surrogate fuel. Examples of design properties include the cetane number (CN), aromatic content, and 90 vol % distillation temperature (T90). A *design property target* is the desired value of a given design property. Examples of property targets corresponding to the design properties above are 43.7 CN, 22 wt % aromatics, and 310 °C T90, respectively. A *surrogate palette* is the set of pure compounds that can be blended together in specified proportions to create a surrogate fuel, and each pure compound in a *surrogate palette* is called a *palette compound*.

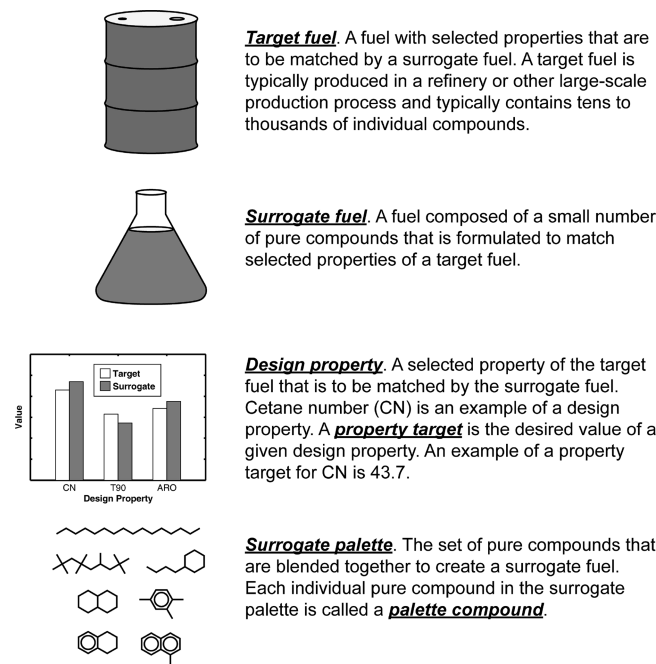
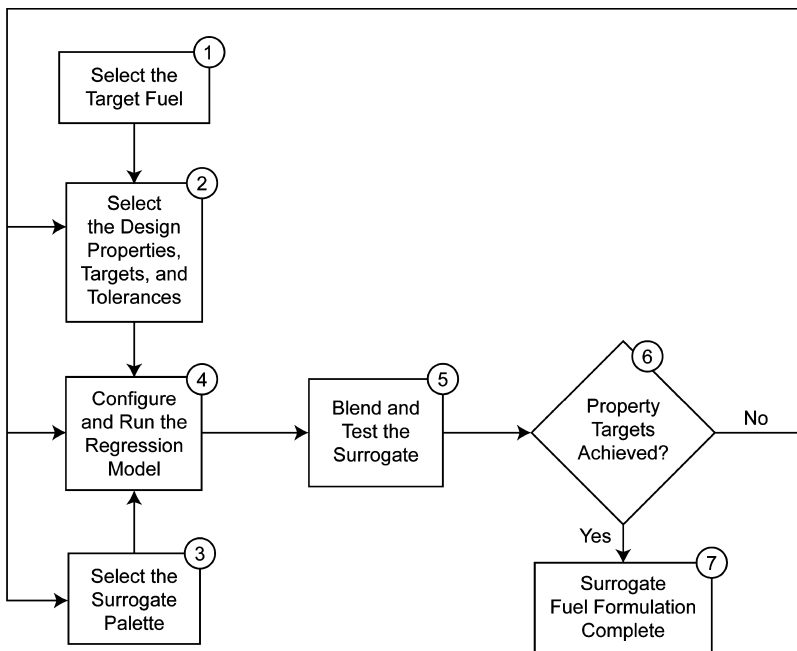


Figure 1. Definitions of terms used in this study.

The approach used in developing diesel surrogate fuels in this study is outlined in Figure 2. The first step was to identify one or more target fuels. Two reference #2 ultra-low-sulfur diesel (ULSD) fuels, described in Section 2.1, were used in this study. Second, the design properties, property targets, and acceptable tolerances on meeting the property targets were established. The design properties selected for this study were fuel composition, ignition quality, volatility, and density. These were selected in an attempt to match the in-cylinder vaporization, mixing, and combustion processes of the target fuel, with the understanding that there is no guarantee that matching these design properties will produce identical engine emissions or performance. Many other potential design properties exist, such as surrogate cost, mean molecular weight, C/H ratio, lower heating value, and threshold sooting index. Cost minimization was not explicitly pursued because palette-compound costs can vary considerably with order quantity, and it was desired to avoid potentially compromising the research value of the surrogates based on this variability. Nevertheless, less-expensive palette compounds were chosen over more-representative but more-costly alternatives when this did not dramatically compromise the ability to formulate surrogates with the desired property-target values. Mean molecular weight also was not explicitly matched, primarily because volatility was considered to be a more accurate and detailed parameter for characterizing the vaporization characteristics of a fuel (see Section 2.3.3). C/H ratio, lower heating value, and smoke point were not explicitly matched because the detailed composition-matching technique employed herein (see Section 2.3.1) was expected to yield surrogates that closely replicate the values of these parameters (see Section 3.5.5).

After the design properties were selected, the surrogate palette was chosen. Ideally each palette compound would be representative of a class of compounds found in the target fuel, and each would have a chemical-kinetic oxidation mechanism available so that its combustion kinetics can be computationally simulated. The surrogate palette used in this study contains representatives from each of the major hydrocarbon families



**Figure 2.** Overview of the process followed to create the surrogate fuels in this study. The order of each step in the sequence is provided in the upper-right region of each box.

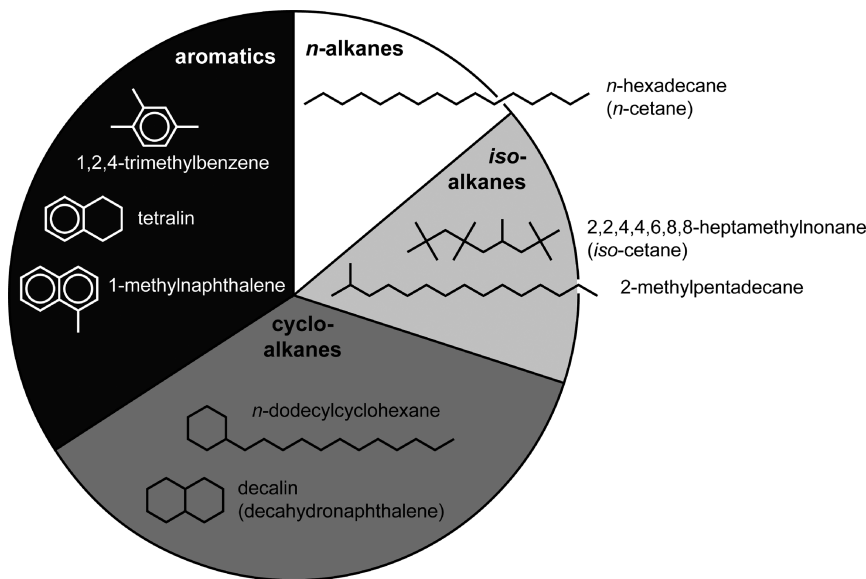


**Figure 3.** Approximate amounts (by mass) of various hydrocarbon classes found in a typical current U.S. #2 ULSD fuel, as well as some potential surrogate compounds to represent each class of hydrocarbons.

found in market diesel fuels: *n*-alkanes, *iso*-alkanes, cyclo-alkanes, aromatics, and naphtho-aromatics. The next step was to identify and run an optimization code to determine the “recipe” for the surrogate, that is, how much of each palette compound should be included in the surrogate to achieve the property targets. The optimization code used in this study is a regression model developed at the National Institute of Standards and Technology (NIST).<sup>25</sup> Once each surrogate composition was determined, the pure palette compounds were blended together to produce the surrogates, and each surrogate was tested to determine whether the property targets were achieved within their desired tolerances. If the property targets were not met, the property targets/tolerances, the regression model assumptions, and/or the surrogate palette could be

adjusted and the process could be iterated until the property targets are met within their specified tolerances. The remainder of this paper is focused on explaining the details and results of each step of this process as it was applied to create surrogates for the two target diesel fuels.

## 2. SURROGATE FUEL FORMULATION METHODOLOGY

This section covers the selection of the target fuels; the techniques used to measure the physical, chemical, and combustion properties (i.e., the design properties) of the fuels; and background on the regression model.

**2.1. Target Fuels.** Two target fuels were selected to illustrate the methodology for formulating diesel surrogate fuels

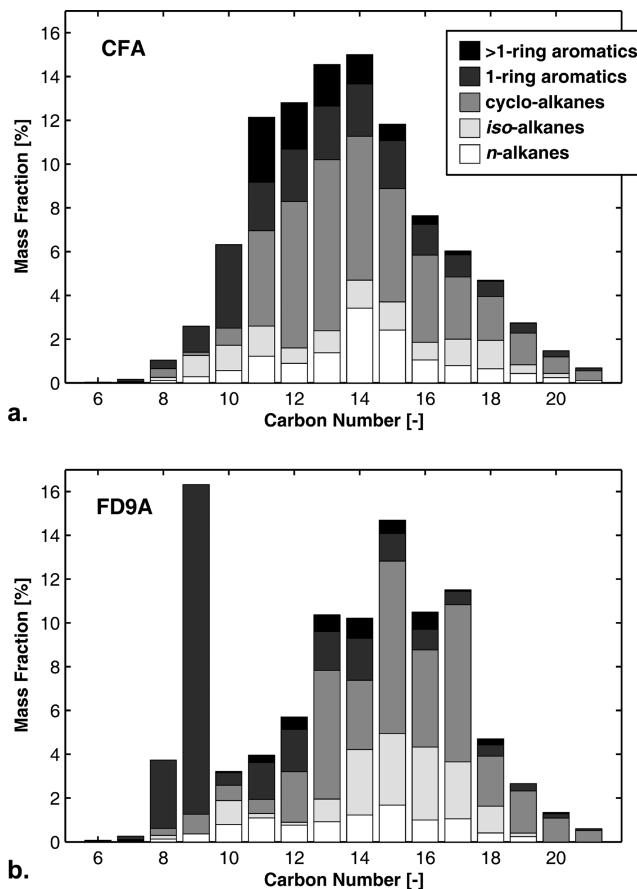
proposed in this study. One of the target fuels was selected from the set of nine Fuels for Advanced Combustion Engines (FACE) reference diesel fuels, which were created and characterized under the auspices of the Coordinating Research Council (CRC) using funding from CRC and the U.S. Department of Energy. The FACE reference diesel fuels were developed to study the effects of fuel-property variations on diesel combustion in engines.<sup>26</sup> FACE Diesel #9 Batch A (FD9A) was selected for use in the present study because it was the most representative of current market diesel fuels. Unfortunately, FD9A also exhibited anomalously high levels of C<sub>8</sub> and C<sub>9</sub> monoaromatics (see Figures 4.27, 4.28, and 6.14 in Alnajjar et al.<sup>26</sup>). Based on this observation, it was decided to use also a 2007 #2 ULSD certification fuel<sup>27</sup> from Chevron-Phillips Chemical Co., denoted in this paper as CFA, as a second target fuel. This fuel showed a more-typical distribution of hydrocarbon class as a function of carbon number (i.e., the number of carbon atoms in a given molecule).

**2.2. Techniques to Measure Fuel Compositional Characteristics.** The detailed compositional characteristics of the target fuel must be known before a surrogate fuel can be created to reproduce these characteristics. A number of ASTM test methods are available for determining the amounts of various hydrocarbon classes in diesel fuel.<sup>28–31</sup> Using these methods, Figure 3 shows the primary hydrocarbon classes and their approximate average mass fractions in a current market #2 ULSD fuel in the U.S.<sup>28,32</sup> The primary hydrocarbon types are *n*-alkanes (saturated straight-chain hydrocarbons), *iso*-alkanes (saturated branched-chain hydrocarbons), cyclo-alkanes (aka naphthenes, saturated hydrocarbons with one or more saturated ring structures), and aromatics (hydrocarbons with one or more benzene ring structures). Compounds with one or more naphthenic and one or more aromatic rings are called naphtho-aromatics. Tetralin is a naphtho-aromatic shown in Figure 3.

While the ASTM test methods referenced above can provide gross compositional information, a number of analytical methods that provide much more detailed diesel-fuel characterization data are emerging. Some of these methods were applied in a study focused on characterizing the FACE reference diesel fuels.<sup>26</sup> One technique used in the FACE diesel characterization study is GC-FIMS (gas chromatography with field ionization mass spectrometry) with PIONA (paraffins, *iso*-paraffins, olefins, naphthenes, and aromatics) analysis. PIONA is a multicolour GC technique that is used to obtain the mass fraction of each hydrocarbon class contained in the target fuel, for compounds with boiling points below 200 °C, while GC-FIMS gives the mass fractions of hydrocarbons with boiling points from 200 to 343 °C.<sup>26</sup>

A bar chart showing the breakdown of hydrocarbon classes from GC-FIMS/PIONA as a function of carbon number for each of the target fuels is presented in Figure 4. The total mass fraction of each hydrocarbon type from the GC-FIMS/PIONA analyses, as well as some additional properties of the target fuels measured using various ASTM methods, are provided in Table 1.

**2.3. Measurement of Surrogate-Design Properties.** The surrogate-design properties selected for use in this study were composition, ignition quality, volatility, and density. Each of these characteristics required measurement as well as uncertainty estimation so that appropriate property targets could be established.

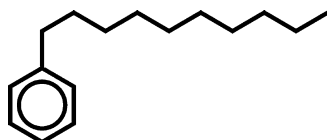


**Figure 4.** Breakdown of hydrocarbon classes by carbon number in the target fuels: (a) CFA; (b) FD9A. Comparison of the distributions shows anomalously high levels of C<sub>8</sub> and C<sub>9</sub> monoaromatics in FD9A, while the CFA distribution is more representative of current #2 ULSD fuels. Data are from GC-FIMS and PIONA analyses conducted at CanmetENERGY.<sup>26</sup> Here and throughout this paper, the “cyclo-alkanes” hydrocarbon class includes compounds with one or more saturated-ring structures but no aromatic rings. The “1-ring aromatics” class includes compounds with one aromatic ring in addition to any other aliphatic (i.e., nonaromatic) structures. The “>1-ring aromatics” class includes compounds with at least two aromatic rings in addition to any other aliphatic structures.

**2.3.1. Compositional Characteristics.** <sup>13</sup>C (carbon) and <sup>1</sup>H (proton) nuclear magnetic resonance (NMR) spectroscopy was selected to quantify the compositional characteristics of each target fuel in this study. While the GC-FIMS/PIONA approach previously discussed was used to select palette compounds with representative carbon numbers, the NMR approach was favored to quantify compositional characteristics because NMR data can yield fuel composition on a *per-carbon-atom* basis, while GC-FIMS/PIONA data are on a *per-molecule* basis. The per-atom data are expected to correlate better with engine emissions characteristics (e.g., sooting propensity) than the per-molecule data because of better resolution of the carbon bond types within each molecule. For example, all of the carbon in *n*-decylbenzene (see Figure 5) would be characterized as “aromatic” in an analysis based on hydrocarbon-molecule class, but an NMR analysis, as employed in this study, would show that only 37.5 mol % of the *n*-decylbenzene carbon is aromatic in character, with the balance having characteristics more representative of alkanes.

Table 1. Selected Properties of the Target Fuels

param.	ASTM test method	CFA	FD9A
density (at 20 °C)	D 4052	848.0 kg/m <sup>3</sup>	846.2 kg/m <sup>3</sup>
cetane number (CN)	D 613	43.3	44.2
derived CN	D 6890	43.7	43.9
distillation	D 86		
initial		178 °C	157 °C
10%		211 °C	184 °C
20%		226 °C	199 °C
30%		235 °C	217 °C
40%		243 °C	238 °C
50%		253 °C	255 °C
60%		261 °C	268 °C
70%		272 °C	281 °C
80%		286 °C	296 °C
90%		310 °C	319 °C
end		342 °C	349 °C
composition	D 1319		
aromatics		25.3 vol %	39.7 vol %
olefins		4.1 vol %	5.1 vol %
saturates		70.6 vol %	56.7 vol %
by GC-FIMS + PIONA			
n-alkanes		13.6 wt %	9.7 wt %
iso-alkanes		11.8 wt %	16.2 wt %
cyclo-alkanes		43.5 wt %	39.3 wt %
1-ring aromatics		21.1 wt %	30.2 wt %
>1-ring aromatics		9.7 wt %	4.5 wt %
aromatics (by SFC)	D 5186		
1-ring		20.7 wt %	32.5 wt %
2 or more rings		9.0 wt %	4.9 wt %
total		29.7 wt %	37.4 wt %
sulfur	D 5453	14.4 mg/kg	3.0 mg/kg
hydrogen	D 5291	13.03 wt %	13.07 wt %
carbon	D 5291	87.04 wt %	86.94 wt %
kin. viscosity (40 °C)	D 445	2.3 mm <sup>2</sup> /s (typ.)	2.11 mm <sup>2</sup> /s
net heat of combustion	D 240	42.90 MJ/kg	42.86 MJ/kg

Figure 5. Molecular structure of *n*-decylbenzene, C<sub>16</sub>H<sub>26</sub>.

A detailed discussion of the application of NMR analyses to the characterization of diesel fuels was provided previously by Pacific Northwest National Laboratory (PNNL) and CanmetENERGY.<sup>26</sup> At CanmetENERGY, the following method was used. NMR analyses were performed at room temperature (19 ± 1 °C) on a Varian Unity Inova 600 NMR spectrometer, operating at 599.733 MHz for proton and 150.817 MHz for carbon. For proton spectra, 20-mg quantities of the diesel samples were dissolved in 700 μL deutero-chloroform, while for carbon spectra, 100-mg quantities in 600 μL deutero-chloroform were used. Both proton and carbon spectra were collected using a Varian 5-mm broadband <sup>13</sup>C{<sup>1</sup>H} probe. No relaxation agent was added.

The quantitative carbon spectra were acquired using an acquisition time of 1.0 s and a sweep width of 36003.6 Hz. A flip angle of 26.0° (3.3 μs) and a relaxation delay of 15 s were used. Reverse-gated waltz proton decoupling was used to avoid nuclear Overhauser effect enhancements of the protonated carbon signals. The spectra were the result of 1600 scans. Line broadening of 3 Hz was used to improve the signal-to-noise ratio of the spectra. The spectra were referenced to the deutero-chloroform being set to 77 ppm.

The quantitative proton spectra were acquired using an acquisition time of 3.0 s and a sweep width of 20000 Hz. A flip angle of 29.6° (3.0 μs) and a relaxation delay of 4 s were used. The spectra were the result of 128 scans. Line broadening of 0.33 Hz was used to improve the signal-to-noise ratio of the spectra. The spectra were referenced to the deutero-chloroform being set to 7.24 ppm.

Distortionless enhancement by polarization transfer (DEPT) spectra were collected using the DEPT pulse sequence provided with the spectrometer with an acquisition time of 1.0 s and a sweep width of 36199.1 Hz. The 90° pulselwidth for carbon was 15 μs, while that for <sup>1</sup>H was 17 μs. A relaxation delay of 1 s was used. Each spectrum was the result of 512 scans. Three spectra were collected for each sample with carbon pulse flip angles of 45°, 90°, and 135°. These three flip angles result in three different spectra, respectively, where all protonated carbon are detected and have positive phase; CH carbons only are detected and have positive phase; and all protonated carbon are detected with CH and CH<sub>3</sub> resonances having positive phase and CH<sub>2</sub> resonances having negative phase. Line broadening of 3 Hz was used to improve the signal-to-noise ratio of the spectra.

At PNNL, 0.05-molar chromium(III) acetylacetone was added as a relaxation agent and slightly different acquisition parameters were used. Nevertheless, there was good reproducibility between the two laboratories, where aromaticity measurements for the same samples were similar within an average difference of ±2.2 mol %.

Both CanmetENERGY and PNNL have developed “carbon type analysis” methods where quantitative proton and carbon NMR spectral integrals and elemental analyses results are used to assign all carbon types using a procedure based on that described by Japanwala et al.<sup>33</sup> For this study, the contents of all carbon types were grouped into 11 carbon types, as described in Section 3.1.1. Due to some differences in carbon-type mole fractions measured for the same target fuel by CanmetENERGY and PNNL, it was decided to average the results from the two laboratories to obtain the carbon-type property targets for each target fuel.

**2.3.2. Ignition Quality.** The derived cetane number (DCN) was selected to quantify the ignition quality of the target fuels, the surrogate mixtures, and the palette compounds in this study. The DCN method was chosen because (1) it is relatively inexpensive to perform, (2) its results correlate well with those obtained using the more-cumbersome engine-based ASTM D 613<sup>34</sup> method, (3) it can be conducted using a sample size as small as 40 mL, and (4) it has high precision. DCN values were measured using the Ignition Quality Tester (IQT) as described in ASTM D 6890-10a.<sup>35</sup> The IQT is a constant-volume combustion device that directly measures the ignition delay (ID) of a fuel injected into an air charge at the method-specified pressure (21.37 bar) and temperature (545 ± 30 °C). The actual charge-air temperature is adjusted as needed to achieve a specified ID of 3.78 ± 0.01 ms for the daily calibration

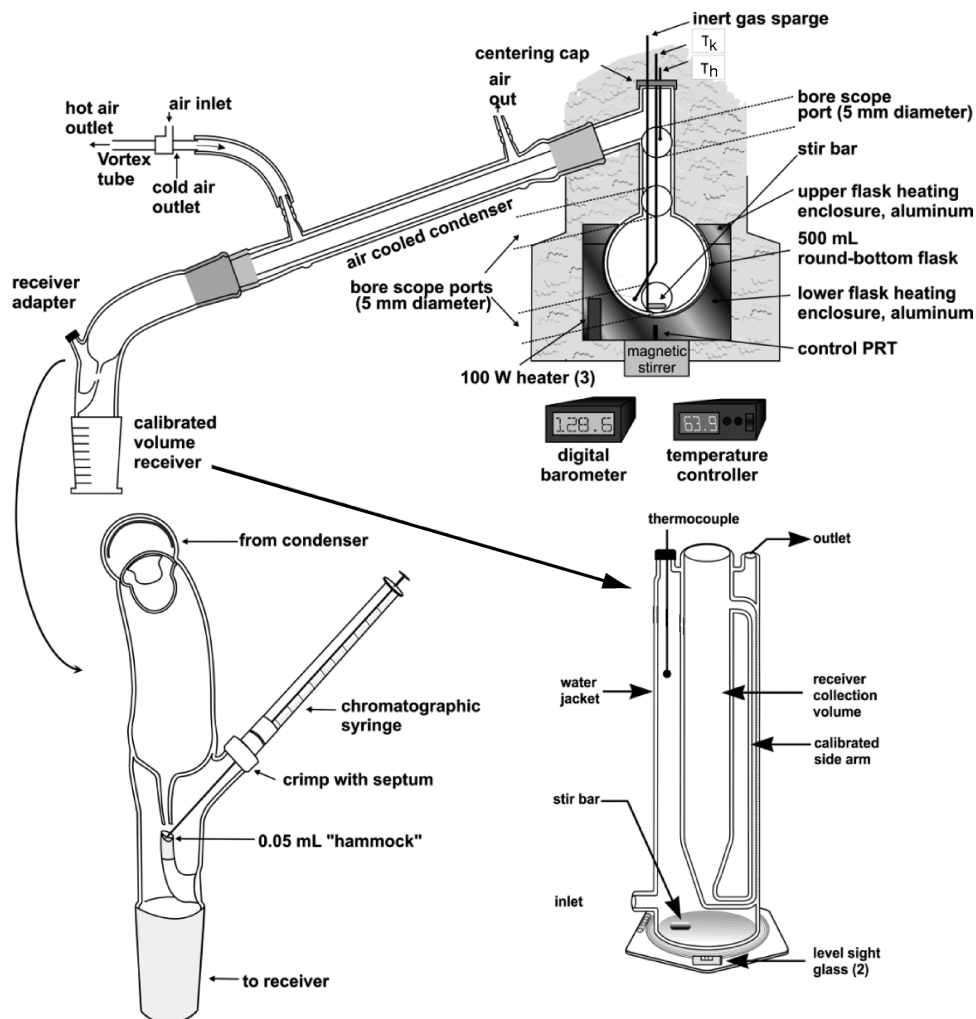


**Figure 6.** Schematic diagram of apparatus used in ADC measurement technique. Expanded views of sampling adapter and stabilized receiver are shown in lower half of the figure.

fuel *n*-heptane. ID is defined from the start of injection (measured by a needle lift sensor) to the point of combustion chamber pressure recovery (measured by a pressure transducer). The ASTM method prescribes 15 injections of the test fuel to stabilize the system, followed without interruption by 32 injections from which the IDs are recorded and averaged. The ID coefficient of variation (COV) for these 32 replicates is typically 1.5–2.5% for hydrocarbons with IDs < 9.5 ms. A trend of increasing COV with increasing ID above ~10 ms has been observed. For example, the measured ID of 2,2,4,4,6,8,8-heptamethylnonane was 21.83 ms with a COV = 5.6%. The average ID from the 32 replicate injections is converted to DCN by one of two equations. For compounds with IDs in the 3.3–6.4 ms range, eq 1 translates to DCNs of 61–34. Equation 2 is used to calculate DCNs for fuels with IDs outside the 3.3–6.4 ms range. The expected reproducibility (for different operators and laboratories using the same sample) for the DCN range of 34–61 is calculated with eq 3. For a 45-DCN fuel, the reproducibility is  $\pm 2.85$  DCN ( $\pm 6.3\%$ ), and 95% of measurements will fall within this range.

$$\text{DCN} (3.3 \text{ ms} < \text{ID} < 6.4 \text{ ms}) = 4.460 + \frac{186.6}{\text{ID}} \quad (1)$$

DCN (ID < 3.3 ms or ID > 6.4 ms)

$$= 83.99(\text{ID} - 1.512)^{-0.658} + 3.547 \quad (2)$$

$$\text{Reproducibility} = 0.0582(\text{DCN} + 4) \quad (3)$$

**2.3.3. Volatility.** The distillation (or boiling) curve is an important property that is measured for complex fluid mixtures.<sup>36,37</sup> Simply stated, the distillation curve is a graphical depiction of the boiling temperature of a fluid or fluid mixture plotted against the volume fraction distilled.<sup>36–38</sup> Distillation curves are typically associated with petrochemicals and petroleum refining,<sup>39</sup> but such curves are of great value in assessing the properties of any complex fluid mixture; indeed, the distillation curve is one of the few properties that can be used to characterize the phase behavior of a complex fluid. Moreover, there are numerous engineering and application-specific parameters that can be correlated to the distillation curve.

The standard test method for atmospheric-pressure distillations, ASTM D 86, provides the usual approach to measurement, yielding the initial boiling point, the temperature at predetermined distillate volume fractions, and the final boiling point.<sup>40</sup> The ASTM D 86 test suffers from several drawbacks, including large uncertainties in temperature

measurements and little theoretical significance. Earlier work has described an improved method and apparatus for distillation curve measurement at atmospheric pressure that is especially applicable to the characterization of fuels and complex mixtures.<sup>41–43</sup> This method, called the advanced (or composition-explicit) distillation curve (ADC) method, is a significant improvement over current approaches. The method features (1) a composition-explicit data channel for each distillate fraction (for both qualitative and quantitative analysis);<sup>44–46</sup> (2) temperature measurements that are true thermodynamic state points that can be modeled with an equation of state;<sup>25,44–49</sup> (3) temperature, volume, and pressure measurements of low uncertainty suitable for equation of state development;<sup>44,45</sup> (4) consistency with a century of historical data;<sup>44,45</sup> (5) an assessment of the energy content of each distillate fraction;<sup>50,51</sup> (6) trace chemical analysis of each distillate fraction;<sup>52,53</sup> and (7) a corrosivity assessment of each distillate fraction.<sup>54</sup> The significant advantage offered by the ADC approach is the ability to develop surrogate mixture models of complex fluids for use with equations of state.<sup>55,56</sup> Such thermodynamic model development is simply impossible with the classical approach to distillation curve measurement, or with any of the other techniques that are used to assess fuel volatility or vapor–liquid equilibrium. This metrology has been applied to azeotropes, gasolines, diesel fuels, aviation fuels, rocket propellants, and crude oils. Moreover, the method also has been applied to the volatility simulation of heavy oils. Herein, the technique is applied to target diesel fuels and their surrogates.

The method and apparatus for the ADC measurement, shown in Figure 6, have been discussed in a number of the sources cited above,<sup>41–46</sup> so additional general description will not be provided here. Samples of the target fuels were stored at 7 °C to preserve any volatile components prior to the ADC measurement. No phase separation was observed as a result of this storage procedure. At the start of each ADC measurement, the required volume of fluid for the measurement (in each case, 200 mL) was placed into the boiling flask with a 200-mL volumetric pipet and an automatic pipetter. The thermocouples were then inserted into the proper locations to monitor  $T_k$ , the temperature in the fluid, and  $T_b$ , the temperature at the bottom of the takeoff position in the distillation head. Enclosure heating was then commenced with a four-step temperature program based on a previously measured distillation curve.<sup>57</sup> This program was designed to impose a heating profile on the enclosure that led the fluid temperature by approximately 20 °C.

During the initial heating of each sample in the distillation flask, the behavior of the fluid was carefully observed. Direct observation through the flask window or through the bore scope allowed measurement of the onset of boiling for each of the mixtures (measured as  $T_k$ ). Temperatures were measured corresponding to three events: the onset of bubbling, sustained bubbling, and vapor-rise into the distillation head. The vapor-rise temperature is important because it is the only point on the distillation curve at which the liquid composition is known. The vapor-rise temperature can be noted visually or by the rapid increase in  $T_b$ , the temperature measured in the distillation head. It has been shown that the vapor-rise temperature is actually the initial boiling temperature of the initial fluid. As the distillation progressed beyond the initial boiling temperature, volume measurements were made in the level-stabilized

receiver, and sample aliquots were collected at the receiver adapter hammock.

Since the measurements of the distillation curves were performed at ambient atmospheric pressure (measured with an electronic barometer), temperature readings were corrected for what should be obtained at standard atmospheric pressure (1 atm = 101.325 kPa). This adjustment was done with the modified Sydney Young equation, in which the constant term was assigned a value of 0.000109.<sup>58,59</sup> This value corresponds to a carbon chain length of 12. Based on the chemical composition of the diesel fuel samples and surrogates, as well as in previous work on diesel fuel, it was found that *n*-dodecane can be used as a surrogate for setting the Sydney Young constant without loss of accuracy in the reported distillation temperatures, since the constant changes slowly with carbon number.<sup>60–63</sup> The magnitude of the correction is dependent upon the extent of departure from standard atmospheric pressure. The location of the laboratory in which the measurements reported herein were performed is approximately 1650 m above sea level, resulting in a typical temperature adjustment of 8 °C. The actual measured temperatures are easily recovered from the Sydney Young equation at each measured atmospheric pressure.

In the course of this study, six complete distillation curve measurements were performed for each of the target fuels, and three for each of the surrogate mixtures. The estimated uncertainty (with a coverage factor  $k = 2$ )<sup>64</sup> in the temperatures is less than 0.3 °C. The uncertainty in the volume measurement that was used to obtain the distillate volume fraction is 0.05 mL in each case. The uncertainty in the pressure measurement (assessed by logging a pressure measurement every 15 s for the duration of a typical distillation) is 0.001 kPa.

**2.3.4. Density.** The last surrogate design property used in this study was density. Target-fuel density was quantified using the procedure described in ASTM D 4052.<sup>65</sup> The densities for the target fuels used in this study are provided in Table 1.

**2.4. Regression Model.** A key challenge in surrogate-fuel formulation is determining the set of palette-compound mole-fractions such that the resultant surrogate mixture best matches the desired properties of the target fuel (i.e., the property targets). In the current study, a regression model was used to provide an automated rather than a manual technique for surrogate formulation. The multiproperty regression algorithm determines the optimal surrogate formulation by matching the surrogate-design properties to the property targets as closely as possible through the use of an objective function. This technique is similar to those employed in previous studies,<sup>25,47–49</sup> but the design properties and implementation are different. The objective function and procedure for running the regression model are described in Section 3.3.

### 3. RESULTS AND DISCUSSION

The first step in using the tools discussed above to formulate surrogate fuels was to establish specifically which surrogate-design properties would be used and to determine how they would be estimated using the regression model.

**3.1.1. Compositional Characteristics.** The NMR techniques described in Section 2.3.1 can provide a quantitative estimate of the mole fraction of each carbon bond type in a fuel. Rather than attempt to match the more than 90 different carbon-bond types quantified using the NMR method, the decision was made to group the results into 11 carbon types that should allow the sooting and other characteristics of different target fuels to be replicated by their respective surrogates. The

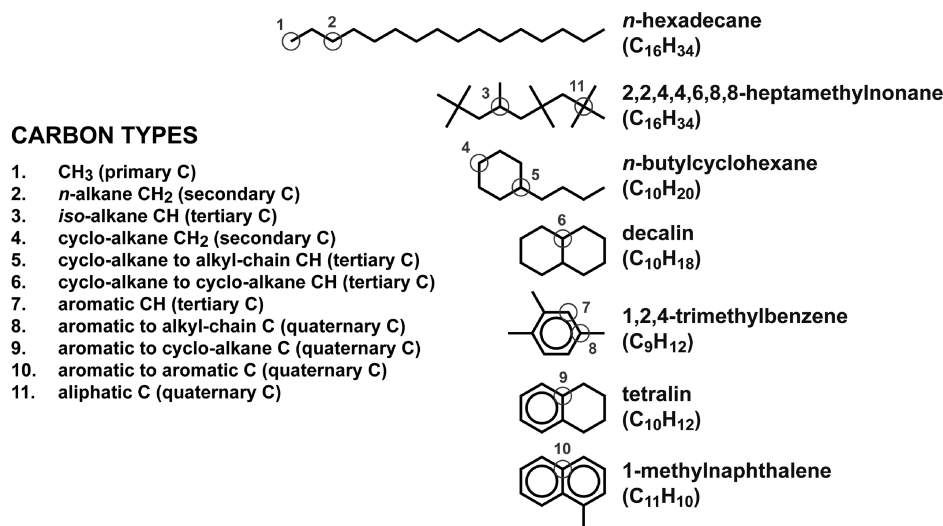


**Figure 7.** Carbon classification system used to match compositional characteristics between target and surrogate fuels. The 11 carbon types (CT) are listed on the left, and an example of each CT is circled in the molecular-structure diagrams on the right.

resultant carbon type (CT) classification system is shown in Figure 7. The NMR data showed that at least 99.7% of the carbon atoms in each target fuel fall into CTs 1–10. This classification system differentiates among the most common CTs found in current diesel fuels (i.e., CTs 2, 4, 1, and 7, in order of decreasing abundance), as well as isolating certain CTs that are expected to correlate with elevated soot emissions (e.g., CTs 9 and 10). CT 11 is a special case because neither of the target fuels contained a measurable amount of it. Rather, CT 11 was included because one of the palette compounds contained a significant fraction of CT 11. The reasons for this are discussed in more detail in Section 3.2. The 11 CTs in Figure 7 were used as the design properties for surrogate composition.

**3.1.2. Ignition Quality.** The surrogate design property selected to quantify ignition quality was the DCN, as measured according to the procedure detailed in ASTM D 6890-10a<sup>35</sup> and described in Section 2.3.2. In the regression model, it was assumed that the DCN of a mixture is equal to the volume-fraction-weighted sum of the DCNs of its constituent compounds, i.e.:

$$\text{DCN} = \sum_{i=1}^{N_{\text{palette}}} v_i \text{DCN}_i \quad (4)$$

where  $i$  is an index spanning the number of palette compounds ( $N_{\text{palette}}$ ), and  $v_i$  and  $\text{DCN}_i$  are the volume fraction of the  $i^{\text{th}}$  component and its DCN, respectively. This assumption was made because it has been shown to be reasonably accurate,<sup>24</sup> and a better relationship that takes into account nonlinear DCN interaction effects for multicomponent mixtures was unavailable.

**3.1.3. Volatility.** The ADC method described in Section 2.3.3 was used to quantify the degree to which the volatility characteristics of the target and surrogate fuels were matched. Whereas the ADC could be measured directly for each of the target fuels and the blended surrogates, the ADC was calculated in the regression model using an equation-of-state-based mixture-model. Any vapor–liquid equilibrium model that is capable of accurately computing a bubble-point temperature for mixtures containing the fluids in the palette can be used to calculate the ADC. In this study, a Helmholtz-based mixing model implemented in the REFPROP program<sup>66</sup> was used to

calculate phase equilibrium, along with a simple, idealized distillation algorithm.<sup>47</sup>

The measured ADC temperatures associated with the initial boiling of the target fuels are provided in Table 2. Comparison

**Table 2. Initial Boiling Behavior of the CFA and FD9A Target Fuels Used in This Study<sup>a</sup>**

obs. temp.	CFA target fuel, $T_k$ [°C] (82.920 kPa)	FD9A target fuel, $T_k$ [°C] (83.154 kPa)
onset	106.6	128.5
sustained bubbling	205.3	193.3
vapor rise	224.4	206.2

<sup>a</sup>Data presented are averages of three separate measurements. Temperatures have been adjusted to 1 atm with the Sydney Young equation; experimental atmospheric pressures are provided in parentheses to allow recovery of actual measured temperatures.

of these results to the ASTM D 86<sup>40</sup> (D86) initial distillation temperatures in Table 1 indicates that while the ADC onset temperature is lower than the D86 initial distillation temperature for each fuel, the sustained-bubbling and vapor-rise temperatures are higher. Furthermore, the sustained-bubbling and vapor-rise temperatures are higher for CFA than for FD9A.

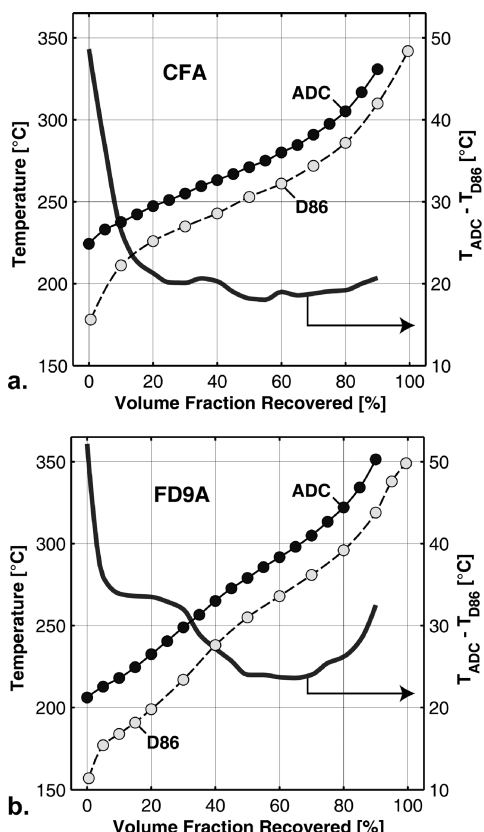
The measured ADC temperatures associated with the bulk distillation of the target fuels are provided in Table 3. These values indicate that there is an appreciable difference in the temperatures measured at the  $T_k$  and  $T_h$  positions across the distillation range for each target fuel. This difference averages approximately 20 °C. The absence of convergence of  $T_k$  and  $T_h$  indicates the absence of azeotropy between the major constituents of the diesel fuel, a result that is consistent with the known literature for petroleum-derived hydrocarbons.<sup>67</sup>

Figure 8 shows the distillation profiles measured using the ADC technique<sup>44</sup> and ASTM D 86<sup>40</sup> for each of the target fuels. The primary difference between the volatilities of the two target fuels is that FD9A begins to boil at a lower temperature than CFA and it requires a higher temperature to complete its distillation, regardless of the technique used to measure the distillation curve. Figure 8 also shows that the ADC kettle temperatures,  $T_k$ , measured directly in the liquid, are

**Table 3. Representative Distillation Curve Data, Given as Averages of Six Complete ADC Measurements for Each Target Fuel in This Study<sup>a</sup>**

distillate vol. frac. [%]	CFA target fuel (82.920 kPa)		FD9A target fuel (83.154 kPa)	
	$T_k$ [°C]	$T_h$ [°C]	$T_k$ [°C]	$T_h$ [°C]
5	233.0	210.0	212.9	192.9
10	237.5	218.5	217.9	198.3
15	242.4	226.1	224.6	206.3
20	247.3	231.9	232.5	213.8
25	251.0	236.3	240.6	221.5
30	255.1	242.2	249.0	229.9
35	259.6	245.0	256.5	236.7
40	263.3	251.7	265.2	242.7
45	267.0	255.4	272.7	250.7
50	271.2	259.4	279.0	258.8
55	275.0	263.8	285.7	268.0
60	280.0	268.9	291.7	274.4
65	284.7	273.4	298.0	279.2
70	290.8	278.9	305.0	283.3
75	297.4	285.7	313.4	291.0
80	305.2	292.5	322.2	296.1
85	316.7	303.2	334.2	306.4
90	330.7	315.9	351.5	319.2

<sup>a</sup>Temperatures have been adjusted to 1 atm with the Sydney Young equation; experimental atmospheric pressures are provided in parentheses to allow recovery of actual measured temperatures.



**Figure 8.** Comparison of distillation temperatures obtained by use of the advanced distillation curve (ADC) and ASTM D 86 (D86) methods for each target fuel: (a) CFA; (b) FD9A. The initial ADC temperature for each fuel is its vapor-rise temperature from Table 2.

consistently higher than the D86 distillation temperatures. The difference between ADC and D86 distillation temperatures for each fuel is shown by the thick solid line and the right-hand y-axis on each plot. This difference is due to the fact that the ADC technique provides thermodynamically consistent temperatures measured in the liquid,<sup>44</sup> whereas D86 provides temperatures measured in the (cooler) vapor above the boiling fuel.<sup>40</sup> A thermodynamically consistent temperature, when associated with a corresponding pressure, constitutes a state point that maps to a fluid density that is consistent with the P- $\rho$ -T surface of a pure compound or mixture.  $T_k$  must be higher than  $T_h$  for mass transfer to occur, but this difference becomes minimal when a pure fluid is vaporized,<sup>68</sup> or when an azeotrope is vaporized.<sup>69</sup> The differences of 20–30 °C across the distillation curve have important implications for palette-compound selection. Specifically, choosing palette compounds based on their normal boiling temperatures being representative of ADC points is preferred, since ADC temperatures and normal boiling temperatures are state points. Choosing palette compounds based on their normal boiling temperatures being representative of D86 points is not advisable, because the lower D86 vapor temperatures would tend to yield a palette that is too volatile.

**3.2. Surrogate Palette Creation.** The surrogate palette used in this study is shown in Figure 9. Some properties of the palette compounds are provided in Table 4, while the number of carbon atoms of each carbon type in each palette-compound molecule is provided in Table 5. Every carbon atom of every palette compound falls into one and only one of the 11 carbon types shown in Figure 7.

Palette compounds were selected based on their ability to represent the types of compounds found in the target fuels, including molecular structures, autoignition properties, boiling and melting points, and densities. In addition, it was desired that each palette compound be commercially available at a purity of >98% for a “reasonable” cost, and there should be a validated detailed chemical-kinetic model available for its oxidation and pyrolysis. The last column of Table 4 shows that detailed chemical-kinetic mechanisms do not yet exist for approximately half of the palette compounds; nevertheless, it is believed that such mechanisms could be available soon. Finally, it was desired to keep the number of palette compounds to the minimum required to adequately match the property targets, in order to minimize the complexity of the detailed kinetic mechanism for each surrogate. It was fairly straightforward to satisfy these simultaneous requirements to identify *n*-alkanes for the palette. Unfortunately, the *iso*-alkanes, cyclo-alkanes, aromatics, and naphtho-aromatics found in the target fuels are challenging (i.e., expensive) to procure in pure form; hence, they have not been well studied. As a result, the selection of palette compounds to represent these hydrocarbon classes was an exercise in balancing trade-offs.

One example of balancing multiple trade-offs was the selection of 2,2,4,4,6,8,8-heptamethylnonane (HMN) as a palette compound. *Iso*-alkanes make up more than 10 wt % of each of the target fuels used in this study (see Table 1 and Figure 3), so they are a major hydrocarbon class. The high-DCN *iso*-alkanes found in refinery diesel fuels typically exhibit light methyl branching near a chain end<sup>12</sup> (e.g., 2-methyltetradecane), but these types of diesel-boiling-range *iso*-alkanes are not currently commercially available in high purity for a reasonable cost. HMN is an *iso*-alkane that is currently commercially available in high purity for a reasonable cost

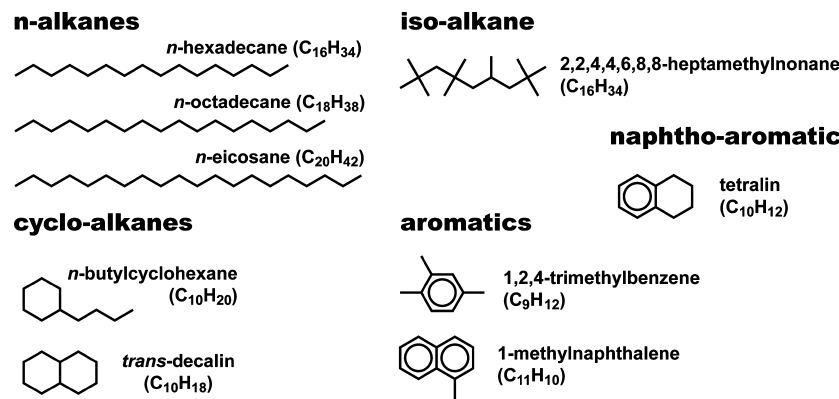


Figure 9. Pure compounds that make up the surrogate palette.

Table 4. Surrogate Palette Compounds and Their Properties

palette cmpd name	abbrev.	CAS #	C	H	mol. wt [g/mol]	MP <sup>a</sup> [°C]	BP <sup>b</sup> [°C]	density <sup>c</sup> [kg/m <sup>3</sup> ]	DCN <sup>d</sup>	purity <sup>e</sup> [wt %]	C–K mech. available?
<i>n</i> -hexadecane	NHxD	544-76-3	16	34	226.4	17.9	286.8	756	100 <sup>g</sup>	99.5	Yes <sup>70</sup>
<i>n</i> -octadecane	NOD	593-45-3	18	38	254.5	27.9	316.8	766	106 <sup>71</sup>	99.0	No <sup>12</sup>
<i>n</i> -eicosane	NEI	112-95-8	20	42	282.5	36.9	343.8	774	110 <sup>71</sup>	99.1	No <sup>12</sup>
heptamethylnonane <sup>f</sup>	HMN	4390-04-9	16	34	226.4		246.4	768	15.1	99.9	Yes <sup>72,73</sup>
<i>n</i> -butylcyclohexane	NBCX	1678-93-9	10	20	140.3	-74.9	183.0	785	47.6	99.9	No <sup>12</sup>
<i>trans</i> -decalin	TDEC	493-02-7	10	18	138.2	-31.2	187.3	851	31.8	99.8	Crude <sup>12</sup>
1,2,4-trimethylbenzene	TMB	95-63-6	9	12	120.2	-46.2	169.4	856	8.9	99.5	Yes <sup>17</sup>
tetralin	TET	119-64-2	10	12	132.2	-35.2	207.7	949	8.9	99.3	No <sup>12</sup>
1-methylnaphthalene	1MN	90-12-0	11	10	142.2	-29.2	244.8	986	0 <sup>g</sup>	95.4	Yes <sup>74–76</sup>

<sup>a</sup>Melting point at 0.10 MPa.<sup>77</sup> <sup>b</sup>Boiling point at 0.10 MPa.<sup>77</sup> <sup>c</sup>From NIST equation of state model at 45 °C and 0.10 MPa. <sup>d</sup>Derived cetane number measured at NREL using ASTM D 6890 unless noted otherwise. <sup>e</sup>Measured at CanmetENERGY by GC × GC-FID/SCD.<sup>78</sup> <sup>f</sup>2,2,4,6,8,8-heptamethylnonane. <sup>g</sup>Defined value.

Table 5. Number of Carbon Atoms of Each Carbon Type in Each Palette-Compound Molecule

palette cmpd name	abbrev.	carbon type (CT)										
		1	2	3	4	5	6	7	8	9	10	11
<i>n</i> -hexadecane	NHxD	2	14	—	—	—	—	—	—	—	—	—
<i>n</i> -octadecane	NOD	2	16	—	—	—	—	—	—	—	—	—
<i>n</i> -eicosane	NEI	2	18	—	—	—	—	—	—	—	—	—
2,2,4,4,6,8,8-heptamethylnonane	HMN	9	3	1	—	—	—	—	—	—	—	3
<i>n</i> -butylcyclohexane	NBCX	1	3	—	5	1	—	—	—	—	—	—
<i>trans</i> -decalin	TDEC	—	—	—	8	—	2	—	—	—	—	—
1,2,4-trimethylbenzene	TMB	3	—	—	—	—	—	3	3	—	—	—
tetralin	TET	—	—	—	4	—	—	4	—	2	—	—
1-methylnaphthalene	1MN	1	—	—	—	—	—	7	1	—	2	—

because it is a diesel primary reference fuel. Nevertheless, HMN is not representative of typical diesel *iso*-alkanes because of its DCN of 15.1, which is uncharacteristically low for a diesel *iso*-alkane, and because of its extreme level of branching. Indeed, 3 of the 16 carbon atoms in HMN exist as quaternary aliphatic carbon (see CT 11 in Figure 7), which was not detected in the target fuels used in this study. The quantitative carbon NMR spectra of the fuels were compared to their carbon NMR spectra collected with the DEPT pulse sequence where only protonated carbons are detected. The two spectra appear to contain all of the same resonances in the aliphatic region, so if quaternary aliphatic species are present, their content is below the limit of detection for the analysis.<sup>79</sup>

If *iso*-alkanes were entirely excluded from the palette, their distillation characteristics could be well approximated by *n*-alkanes, but that would eliminate all sources of CT 3 (tertiary

alkane carbon, see Figure 7), a CT that comprises ~5 mol % of the target fuels used in this study. Also, *n*-alkanes have shorter ignition delays (and hence larger cetane numbers) than *iso*-alkanes of the same carbon number,<sup>71,80</sup> and all of the low-DCN compounds in the palette (except HMN) also have low carbon numbers. Finally, *n*-alkanes in the C17 and higher range tend to be solids at typical ambient conditions, which could cause problems if they were to crystallize out of a blended surrogate fuel. Hence, HMN was selected as the sole *iso*-alkane palette compound, primarily due to the existence of a detailed kinetic mechanism, its commercial availability in high purity for a reasonable cost, its simultaneous low CN and high carbon number, and the lack of alternative *iso*-alkane candidates.

In selecting cyclo-alkanes, aromatics, and a naphtho-aromatic for the palette, the common theme was that the palette compounds are generally of too low a molecular weight to be

truly representative of the most prevalent compounds in these chemical classes that are found in market diesel fuels. Nevertheless, the compounds were selected because they were the species with the highest molecular weights that are available in high purity for a reasonable cost, and for which kinetic mechanisms exist. For the cyclo-alkanes, *n*-butylcyclohexane was selected as the representative monocycloalkane; it is the only source of CT 5. Decalin was selected as the representative dicycloalkane; it is the only source of CT 6. There are two stereoisomers of decalin: *cis* and *trans*. Because the palette was generally lacking in low-CN compounds, *trans*-decalin (DCN = 31.8, see Table 4) was chosen in favor of *cis*-decalin (DCN = 41.6).<sup>81</sup> The representative monoaromatic was chosen to be 1,2,4-trimethylbenzene, in part, as a result of its abundance in a detailed hydrocarbon analysis of FD9A.<sup>82</sup> Tetralin was selected as the representative naphtho-aromatic for the palette. Tetralin is the only source of CT 9. 1-methylnaphthalene (1MN) was selected as the representative diaromatic compound, in part, on the basis of its past use as a diesel primary reference fuel, and because, unlike naphthalene, 1MN is a liquid at standard conditions. 1MN is the only source of CT 10.

Many additional palette compounds were considered during the course of this study, but they were excluded from the final palette for one or more of the following reasons: (1) they were not selected by the regression model for inclusion in the final surrogates; (2) they were not available in high purity for a reasonable cost; (3) a detailed chemical-kinetic oxidation mechanism for the compound was not available or planned for development; or (4) a similar compound with more desirable characteristics was available. Care was taken to keep the number of palette compounds as small as possible while still representing the major hydrocarbon classes in the target fuels. Compounds could not be eliminated from the final palette shown in Figure 9 without losing the single representative of an important hydrocarbon type or sacrificing the ability to match property targets (e.g., two high-carbon-number *n*-alkanes are needed to match the heavy end of the distillation curve without excessively increasing the DCN error).

Once the palette compounds were identified, they were procured from commercial sources. Upon receipt, the compounds were analyzed to verify that their respective specified purities had been met and to characterize any significant impurities (see Table 4).<sup>78</sup> The compounds had purities of 99.0 wt % or greater except for 1MN. This compound was found to have a purity of 95.4 wt %, where the major contaminants were isomers of methylbenzothiophene, a sulfur-containing compound. The 4.2 wt % methylbenzothiophene level in the 1MN<sup>78</sup> yields sulfur contents of 990 and 400 ppm (by weight) in the CFA and FD9A surrogates, respectively. Further purification of the 1MN to remove the methylbenzothiophenes was investigated but not implemented for the following reasons: (1) it would greatly increase the cost of the 1MN; (2) the contamination did not substantially affect the CT mole fractions, DCN, or volatility characteristics of the 1MN; and (3) making the surrogates compatible with sulfur-sensitive aftertreatment systems on production engines was not deemed worth the significant additional cost at this stage of the surrogate-development process. Nevertheless, the elevated sulfur levels of the surrogates could lead to higher engine-out PM emissions due to increased sulfate in the exhaust.<sup>83</sup>

### 3.3. Regression Model Objective Function and Computations.

The objective function that was minimized in the regression model is defined as follows:

$$S = \sum_{i=1}^{N_{CT}} W_{i,CT} F_{i,CT}^2 + W_{DCN} F_{DCN}^2 + \sum_{i=1}^{N_{ADC}} W_{i,ADC} F_{i,ADC}^2 + W_{\rho} F_{\rho}^2 \quad (5)$$

where  $S$  is the function to be minimized, each  $W$  is a weighting factor, and each  $F$  is a normalized difference between a design-property target and the corresponding design-property value calculated in the regression model. Beyond the quantitative minimization of  $S$  achieved by the regression model, values for the weighting factors can be adjusted as desired through a trial-and-error procedure to achieve a qualitative "best match" between surrogate and target-fuel characteristics. Each of the four terms on the right-hand side of eq 5 corresponds to a design property, as indicated by its subscript: CT denotes carbon type, DCN denotes derived cetane number, ADC denotes advanced distillation curve, and  $\rho$  denotes density. In the first summation in eq 5, the index  $i$  runs over all of the carbon types,  $N_{CT}$ , while in the second summation it runs over all of the ADC points,  $N_{ADC}$ . Summation is unnecessary in the DCN and  $\rho$  terms because each fuel has only one DCN and one  $\rho$ . The normalized difference terms in eq 5 are defined as follows:

$$F_{i,CT} = 100 \frac{CT_{i,calc} - CT_{i,meas}}{CT_{i,meas}} \quad (6)$$

$$F_{DCN} = 100 \frac{DCN_{calc} - DCN_{meas}}{DCN_{meas}} \quad (7)$$

$$F_{i,ADC} = 100 \frac{ADC_{i,calc} - ADC_{i,meas}}{ADC_{i,meas}} \quad (8)$$

$$F_{\rho} = 100 \frac{\rho_{calc} - \rho_{meas}}{\rho_{meas}} \quad (9)$$

In eqs 6 and 8, each  $CT_i$  is the mole fraction of a given carbon type, and each  $ADC_i$  is the temperature in Kelvins of a given point on the advanced distillation curve. In eqs 7 and 9, DCN and  $\rho$  denote derived cetane number and density values, respectively.

Using the surrogate palette shown in Figure 9, the regression model was initialized with a mixture containing all palette compounds in equal amounts and an initial set of weighting factors. It was then run iteratively to determine a surrogate-fuel formulation that would match the 11 carbon types in its corresponding target fuel as closely as possible, while simultaneously matching the DCN to within 1.5 of the value shown in Table 1, each point on the advanced distillation curve shown in Figure 8 to within  $\pm 7$  °C, and fuel density to within 5% of the value shown in Table 1. Since it was unknown at the beginning of the regression exactly how each weighting factor for each design property would affect the surrogate composition obtained and the resulting agreement with the property targets, the process to determine the best set of weighting factors was iterative. An initial set of weighting factors was chosen, and the regression was run to yield a surrogate formulation that best matched the property targets with these weighting factors. If a particular property target was not met to within the desired tolerance, the weighting factor for

the corresponding surrogate-design property was increased to facilitate improved matching in the next iteration. The final weighting factors on carbon type, cetane number, advanced distillation curve points, and density for the CFA surrogate were 30, 2000, 8000, and 1, respectively. These weights provided the best overall match to the CFA target-fuel properties. In the same order, the weighting factors that were obtained to create the FD9A surrogate were 20, 3000, 9000, and 1.

A final constraint was imposed on the regression model, with the goal of better matching the sooting propensity of the target fuel by preventing very high levels of CT 9 and/or CT 10. Specifically, if the mole fractions of CT 9 and/or CT 10 yielded in an iteration of the regression model for a given surrogate were higher than the corresponding CT mole fractions in the corresponding target fuel, then the mole fractions of tetralin and/or 1-methylnaphthalene were decreased so that the surrogate had the same mole fractions of CT 9 and/or CT 10 as the target fuel. Then, the iterations were continued with the tetralin and/or 1-methylnaphthalene mole fractions pegged at their respective maximum allowable values. For both surrogates reported here, the restriction on CT 10 was necessary.

**3.4. Surrogate Compositions.** The composition of each of the surrogate fuels formulated using the above procedure is given in Figure 10, where the palette-compound name

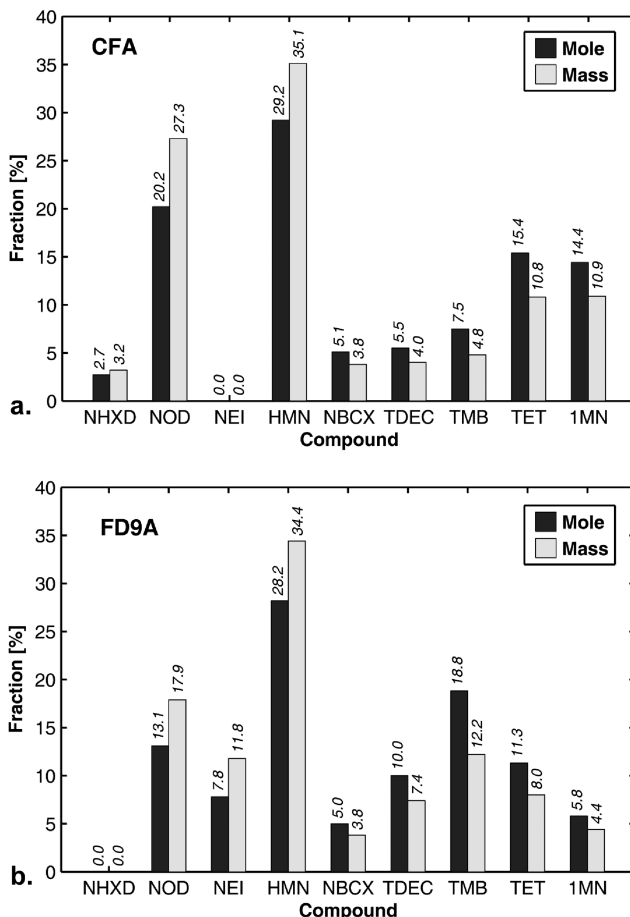


**Figure 10.** Surrogate-fuel compositions by mole and by mass: (a) CFA; (b) FD9A. The number above each bar is the numerical value corresponding to the bar height.

abbreviations are as defined in Table 4. Only two of the three *n*-alkanes were used in each of the surrogates, but all of the other compounds were used, so each surrogate was composed of eight pure compounds. The mass of each palette compound in each surrogate was calculated using the mass fractions from the regression model (see Figure 10), and the surrogates were blended gravimetrically using a commercial electronic balance with 0.1-g resolution. Tare weights for the 1-L brown glass bottles were recorded and the balance was zeroed after each compound was added and its mass recorded. The headspace of each bottle was gently purged with nitrogen and sealed with a Teflon-lined cap after blending. No visible liquid–solid or liquid–liquid separation during long-term storage at room temperature has been observed in either blended surrogate. The approximate cost of each blended surrogate was \$370/L or \$1400/gal (cost of palette compounds only).

### 3.5. Degree to Which Surrogate Fuels Achieve Desired Property Targets.

In the results presented below, the following abbreviations will be used: MT for measured properties of a target fuel, PS for predicted properties of a surrogate fuel (from the regression model), and MS for measured properties of a blended surrogate fuel.

**3.5.1. Compositional Characteristics.** The breakdown of each surrogate and target fuel by mole fraction of each carbon type is shown in Figure 11. The bars labeled MT are the values

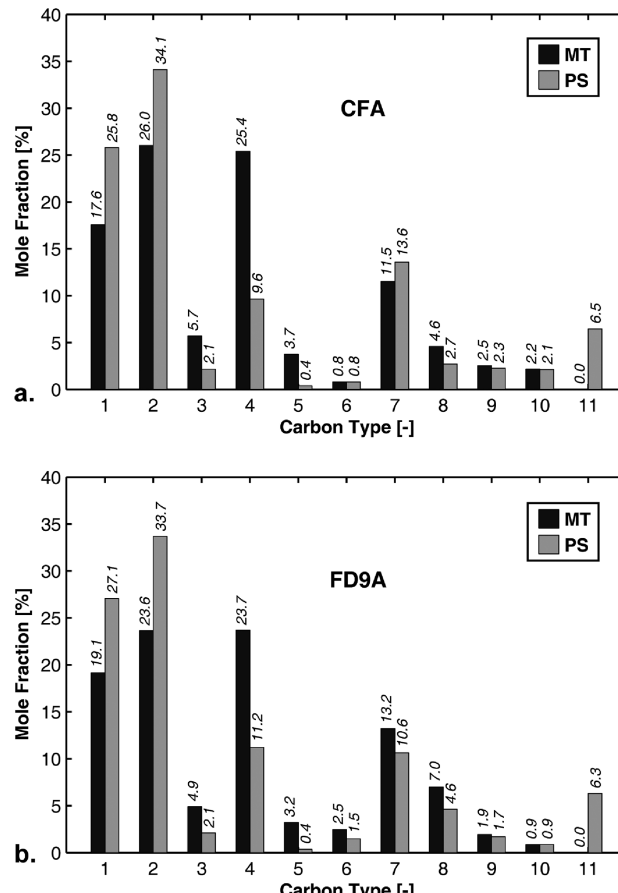


**Figure 11.** Comparison of target- and surrogate-fuel compositional characteristics as quantified by carbon type (see Figure 7 for carbon-type definitions): (a) CFA; (b) FD9A. The number above each bar is the numerical value corresponding to the bar height.

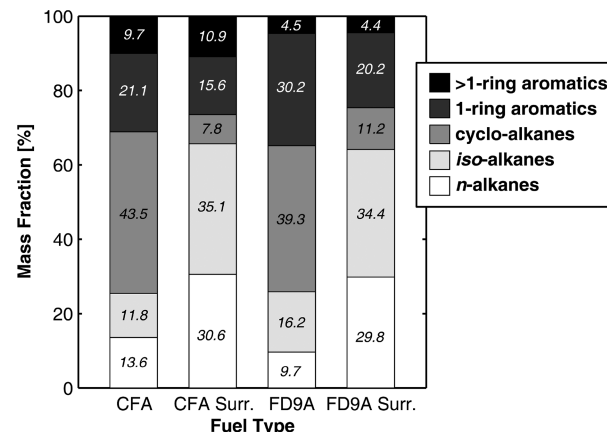
measured for each target fuel by NMR carbon-type analysis. Each bar has an estimated uncertainty of  $\pm 3$  mol %.<sup>26</sup> The bars labeled PS are the values for the corresponding surrogate. The PS values were calculated from the known mole fraction of each palette compound in each surrogate (from Figure 10) and the known mole fraction of each carbon type in each palette compound (from Table 5). Agreement between MT and PS values is within the uncertainty of the MT value for CTs 6–10 for both fuels, showing that the dicycloalkane, monoaromatic, naphtho-aromatic, and diaromatic carbon mole fractions are well-matched.

The match between MT and PS is not as close for CTs 1–5 and 11 as it is for CTs 6–10. Each surrogate contains too much of CTs 1, 2, and 11, and too little of CTs 3, 4, and 5. The high levels of CTs 1 and 2 indicate that the surrogates have primary and secondary alkane carbon mole fractions that are too high. The high levels of CT 2 in particular would be expected to lead to DCNs above the target values. The low levels of CT 3 show that the surrogates do not have enough tertiary alkane carbon; that is, the surrogates do not have enough lightly branched iso-alkane character. The low levels of CTs 4 and 5 indicate that the surrogates have too little cyclo-alkane carbon. The excessively high levels of CT 11 (quaternary carbons) are not surprising because, as discussed above, neither of the target fuels contained a measurable amount of CT 11. The moderate amounts of CT 11 come from the relatively large fractions of HMN in each of the surrogate fuels, as shown in Figure 10, which arise from the need to lower the CNs of the surrogates without excessively increasing their light-end volatilities or aromatic contents.

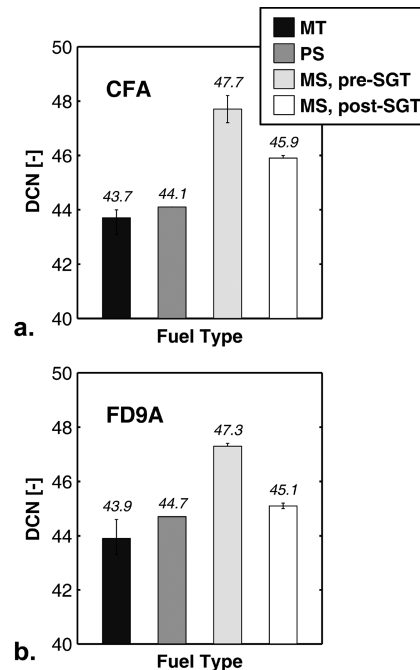
One way to quantify the compositional fidelity of a surrogate fuel is to compare its CT mole fractions to the corresponding CT mole fractions of the target fuel, as discussed above. Indeed, this was the approach employed in the regression model to achieve the best possible compositional fidelity in the presence of the other optimization constraints. An alternative way to assess compositional fidelity is to compare the mass fraction of each hydrocarbon class between the target and surrogate fuels. This type of comparison is possible in the present study by using the GC-FIMS and PIONA data from Table 1 for the target fuels and the palette-compound mass fractions from Figure 10 for the surrogate fuels. The results are shown in Figure 12.

Figure 12 shows that the surrogates have *n*- and iso-alkane mass fractions that are each at least twice as large as their corresponding target-fuel values, while the cyclo-alkane and monoaromatic mass fractions of the surrogates are at least 70% and 25% smaller, respectively. The mass fraction of aromatics with more than one ring is well matched between each surrogate and its corresponding target fuel. Though the CT-mole-fraction and hydrocarbon-mass-fraction approaches for quantifying compositional characteristics are significantly different (the former measures specific carbon-bond characteristics whereas the latter measures gross hydrocarbon classes) some of the overall conclusions are similar. The surrogate fuels generally have too much *n*-alkane character, too much HMN, and not enough cyclo-alkane character. In addition, the observation that the cyclo-alkane and monoaromatic mass fractions are too low while the corresponding CT mole fractions are well-matched indicates that the molecular weights of the cyclo-alkane and monoaromatic compounds in the palette are too low.

**3.5.2. Ignition Quality.** The DCNs for the target and surrogate fuels are shown in Figure 13. At least two replicates of



**Figure 12.** Comparison of target- and surrogate-fuel compositions by mass fraction of each hydrocarbon class. In general, the cyclo-alkane and monoaromatic contents of the surrogates are too low, while the *n*- and iso-alkane contents are too high.



**Figure 13.** Comparison of target- and surrogate-fuel ignition-quality characteristics as quantified by DCN (derived cetane number): (a) CFA; (b) FD9A. MT = measured value for target fuel; PS = predicted value for surrogate fuel from regression model; MS, pre-SGT = measured value for surrogate fuel blended from palette compounds that did not undergo SGT (silica-gel treatment); MS, post-SGT = measured value for surrogate fuel made from palette compounds that separately received SGT prior to blending. At least two replicates of each DCN measurement were made. Bar height indicates mean measured DCN, the numerical value of which is given above each bar. Each error bar indicates minimum and maximum measured DCN values.

each DCN measurement were made. Ignoring the MS values for the moment, in general, the PS values from the regression model are higher than the corresponding MT DCNs. This is believed to be caused by the relatively high levels of heavy *n*-alkanes with high DCNs (see Table 4) that are required to accurately reproduce the heavy end of the distillation curve. In other words, the increase in DCN that corresponds to matching

the heavy end of the distillation curve cannot be completely offset by adding low-DCN components at the light end of the distillation curve without excessively increasing the corresponding volatility and composition errors in the regression-model objective function (eq 5).

Returning to the MS values, it is evident from Figure 13 that the “MS, pre-SGT” values, that is, the measured values obtained after simply blending the surrogates from the “pure” palette compounds, are  $\sim 3$  DCN higher than the PS values. This error was deemed significant because it is larger than the DCN tolerance of 1.5 that was established at the start of this study, larger than the  $\pm 0.85$  DCN repeatability of the ASTM D 6890 technique,<sup>35</sup> and potentially large enough to cause changes in HC, CO, and/or PM emissions of  $>10\%$  in engine tests.<sup>83</sup>

Three potential causes for the higher-than-expected MS DCN values were identified: (1) contamination of one or more palette compounds with one or more ignition-promoting species, (2) uncertainties in pure-compound DCNs, and (3) inadequate accuracy of the volumetric linear-blending assumption for DCN (i.e., eq 4). Each of these potential causes was investigated separately.

The potential for contamination of one or more palette compounds with one or more ignition-accelerating species seemed perhaps the most likely cause of the higher-than-expected MS DCN values, since this mechanism has been observed by others.<sup>84,85</sup> In particular, passing a sample of methylcyclohexane with a higher-than-expected DCN through a column of baked silica gel was found to return the DCN of the sample to its expected range.<sup>84</sup> Due to this documented success, it was decided to try this approach in the current study. The process of gravity-feeding a sample through an open chromatography column of oven-dried silica gel is called silica-gel treatment (SGT).

SGT was first run on each blended surrogate, but the post-SGT measured DCN value for the FD9A surrogate (not shown in Figure 13) was found to be higher than the pre-SGT value. This unexpected result is believed to be due to the preferential evaporative loss of one or more high-volatility, low-DCN components of the surrogate (e.g., TMB) during the  $\sim 5$  h required for the surrogate to gravity-feed through the open column. Hence, it was decided to separately treat each palette compound and then mix them so that the lighter, low-DCN fuel components would not be lost preferentially. A fresh packing of silica gel was used for each compound according to the procedure developed for stabilizing the ignition delay of methylcyclohexane.<sup>84</sup> Because *n*-octadecane and *n*-eicosane are solids at room temperature, partial blends of the appropriate *n*-alkanes were prepared in HMN, and these alkane solutions were then purified via SGT. GC-FID analysis of the *n*- and *iso*-alkane preblends before and after SGT confirmed that the relative proportions of their constituent compounds did not change as a result of SGT. The purified *n*- and *iso*-alkane preblends were subsequently blended with the other purified palette compounds to create the corresponding surrogate fuels. The measured DCN values for the surrogates that were blended after separately running the SGT on the *n*-/*iso*-alkane preblends and the other individual components are denoted “MS post-SGT” in Figure 13. The differences between the MT, MS pre-SGT, and MS post-SGT values and the PS value for each fuel are shown in Figure 14.

Figures 13 and 14 show that running the SGT on the *n*-/*iso*-alkane preblends and the other palette compounds separately before blending the surrogates was effective at bringing the MS

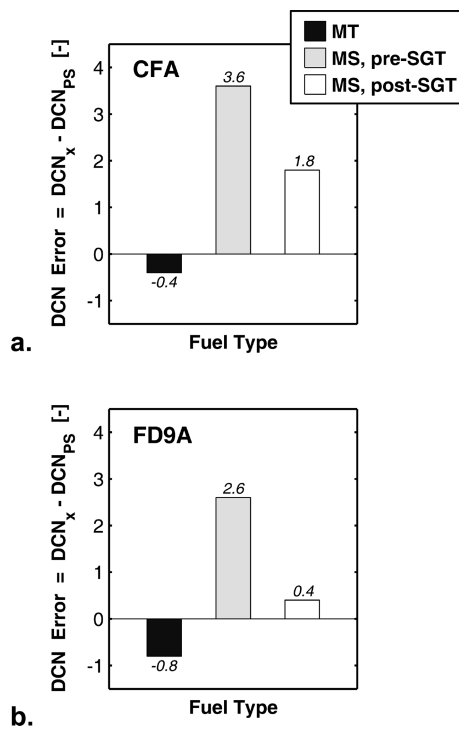


**Figure 14.** Difference between measured DCN of given fuel type and predicted value for surrogate fuel from regression model: (a) CFA; (b) FD9A. Results show that SGT is effective at lowering measured DCN of each surrogate so that it is closer to predicted value derived from assumption that DCN blends linearly with volume fraction and DCN of each palette compound in the mixture (i.e., eq 4). MT; MS, pre-SGT; and MS, post-SGT definitions are provided in Figure 13 caption. Number near each bar end is numerical value corresponding to bar height.

DCN values closer to their respective PS values. Based on this result, it appears that at least one of the palette compounds was contaminated with one or more ignition-accelerating species (likely peroxides) that were removed by SGT. While it is not known exactly which palette compounds were contaminated, pre- and post-SGT measured DCNs for *n*-hexadecane (NHXD) were 119 and 96, respectively, indicating that at least the NHXD was contaminated. Sparging the contaminated NHXD with nitrogen gas for 8 h to remove air from the sample had no measurable effect on the DCN. Also, running the SGT on only the *n*-/*iso*-alkane preblends did not reduce the MS DCNs as much as running the SGT on the *n*-/*iso*-alkane preblends and each of the remaining liquid palette compounds separately, suggesting that palette compounds in addition to the *n*- and *iso*-alkanes also contained ignition-accelerating contaminants. The identities and concentrations of the ignition-accelerating contaminants were not determined, but there are reports that a few tens of parts per million of naturally produced peroxides<sup>85</sup> can lead to changes in the ignition delay and DCN similar in magnitude to the changes seen in this study, and that molecular-sieve material can be effective at removing these peroxides.<sup>86</sup> Several important unresolved questions remain regarding how silica-gel adsorption characteristics change with volume of processed sample. Efforts are currently underway to answer these questions, and it is anticipated that results will be reported in a future publication.

Uncertainty in individual palette-compound DCNs is another potential explanation for the higher-than-expected

MS post-SGT DCN values. It was not possible to directly measure the DCNs of the solids NOD and NEI, so they were assigned values taken from the literature.<sup>71</sup> These assigned DCNs are therefore subject to measurement-system biases relative to the IQT. For high-DCN compounds, a small change in ignition delay can produce a large change in DCN (see eq 2), so uncertainties in the *n*-alkane DCNs could play a role in explaining the higher-than-expected DCNs of the surrogates. Furthermore, 1MN would not autoignite in the IQT under the prescribed ASTM D 6890 operating conditions. Since 1MN is also a primary reference fuel, it was assigned a DCN equal to its defined value of 0. The other very-low-DCN compounds, TMB and TET, had long ignition delays (~67 ms) with large coefficients of variation of 30% and 10%, respectively. Consequently, there is increased uncertainty in the accuracy of the DCN values used for these compounds as well.

A third potential source of differences between PS and MS DCN values is inadequate accuracy of the assumption that the DCN of a mixture is equal to the volume-fraction-weighted sum of the individual palette-compound DCNs (i.e., eq 4). To assess this possibility, alternative mass- and mole-fraction-weighted linear-blending assumptions were evaluated. Figure 15 shows the results of replacing the volume-fraction term in eq 4 with a mole- or mass-fraction term, compared to the MS post-SGT DCN values. These results show that the volume-fraction-weighted linear-blending model in eq 4 provides a better estimate of the MS post-SGT DCN than the alternatives.

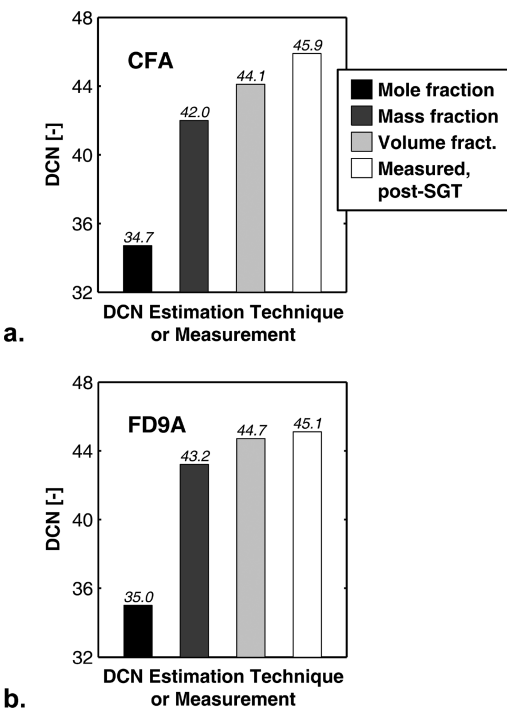


**Figure 15.** Surrogate DCN values predicted assuming linear blending based on mole-, mass-, and volume-fraction-weighted palette-compound DCN values, respectively, compared to measured surrogate DCN when surrogate blended after separately running SGT on individual liquid palette compounds or preblends as described in the text: (a) CFA; (b) FD9A. Results indicate that volume-fraction-weighted blending assumption gives predictions that are closest to measured values. The number near each bar end is the numerical value corresponding to the bar height.

Nonlinear blending effects could be important as well, but these were not investigated in this study.

**3.5.3. Volatility.** Figure 16 shows the MT, PS, and MS ADC data on the left-hand *y*-axis and the difference between the MT

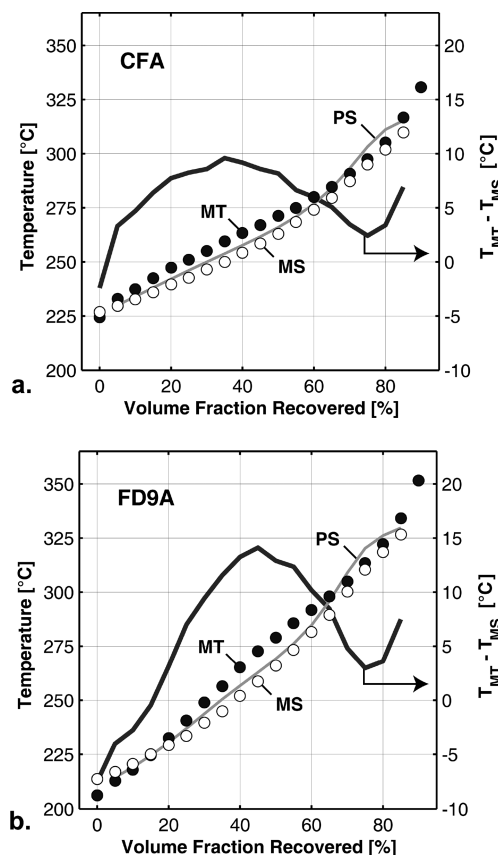


**Figure 16.** Comparison of target- and surrogate-fuel volatility characteristics as quantified by the advanced distillation curve: (a) CFA; (b) FD9A. Left-hand *y*-axis corresponds to MT, PS, and MS distillation values; right-hand *y*-axis corresponds to difference between MT and MS ADC values.

and MS values on the right-hand *y*-axis. The ADC for each blended surrogate was measured by employing the same procedure that was used for the target fuels, and the MS data are provided in Tables 6 and 7 (the corresponding MT values are available in Tables 2 and 3). Table 6 shows that the surrogate fuels tend to have higher onset, sustained-bubbling, and vapor-rise temperatures than their corresponding target

**Table 6. Initial Boiling Behavior of the CFA and FD9A Surrogate Fuels Used in This Study<sup>a</sup>**

obs. temp.	CFA surrogate $T_k$ [°C] (83.65 kPa)	FD9A surrogate $T_k$ [°C] (83.83 kPa)
onset	207.3 (100.7)	141.8 (13.3)
sustained bubbling	225.0 (19.7)	211.5 (18.2)
vapor rise	226.8 (2.4)	213.7 (7.5)

<sup>a</sup>Data presented are averages of three separate measurements. Temperatures have been adjusted to 1 atm with the Sydney Young equation; experimental atmospheric pressures are provided in parentheses to allow recovery of actual measured temperatures. Increases relative to target-fuel measurements from Table 2 are shown in pointed brackets.

**Table 7. Representative Distillation Curve Data, Given as Averages of Three Complete ADC Measurements for Each Surrogate Fuel in This Study<sup>a</sup>**

distillate vol. frac. [%]	CFA surrogate fuel (83.65 kPa)		FD9A surrogate fuel (83.83 kPa)	
	T <sub>k</sub> [°C]	T <sub>h</sub> [°C]	T <sub>k</sub> [°C]	T <sub>h</sub> [°C]
5	229.7	214.8	216.9	203.2
10	232.8	216.0	220.7	206.8
15	236.0	220.5	225.1	210.3
20	239.6	225.6	229.4	211.9
25	242.7	228.7	233.6	215.4
30	246.5	232.4	239.6	221.2
35	250.0	235.3	244.9	226.5
40	254.1	242.1	251.9	233.4
45	258.4	245.4	258.6	237.5
50	263.0	248.4	266.1	245.5
55	268.4	254.1	273.3	252.1
60	274.0	260.8	281.5	258.3
65	279.6	266.8	289.5	264.7
70	287.3	275.3	300.2	272.9
75	295.0	280.3	310.4	277.1
80	301.8	285.0	318.6	286.3
85	309.8	297.4	326.7	300.4
90	313.7	303.9	330.7	311.9

<sup>a</sup>Temperatures have been adjusted to 1 atm with the Sydney Young equation; experimental atmospheric pressures are provided in parentheses to allow recovery of actual measured temperatures.

fuels; that is, the surrogates are less volatile at their light ends. These differences, including the 100.7 °C increase in onset temperature for the CFA surrogate relative to its target-fuel value, are believed to be due to small amounts of high-volatility components in the target fuels. In contrast, the surrogates tend to have lower ADC temperatures across the rest of the distillation range, as shown in Figure 16. The surrogates generally replicate the distillation characteristics of their corresponding target fuels to within 10–15 °C, and the desired ADC matching of ±7 °C over the full distillation range was not achieved for either fuel. The ADC differences shown on the right-hand *y*-axis of Figure 16 are generally lower at the start and end of the distillation curve, and peak in the 30–55 vol% recovered range. This is consistent with the observation from Table 4 that the palette contains no compounds with boiling points from 247 to 286 °C, a temperature range that corresponds to the 30–55 vol% recovered range for the target fuels.

**3.5.4. Density.** The predicted densities of the CFA and FD9A surrogates at 20 °C are 817 kg/m<sup>3</sup> and 808 kg/m<sup>3</sup>, respectively. Compared to the property targets shown in Table 1, it is evident that the densities for the CFA and FD9A surrogates are 3.7% and 4.5% lower, respectively. These errors are within the desired 5% tolerance for density. The lower densities for the surrogates are consistent with their *n*- and *iso*-alkane contents being too high, since *n*- and *iso*-alkanes generally have lower densities than molecules of similar carbon number in other hydrocarbon classes (see Table 4).

**3.5.5. Other Parameters.** The molar C/H ratio, net heat of combustion (aka lower heating value), and smoke point were measured or calculated for each of the target and surrogate fuels, and the results are provided in Table 8. Although the molar C/H ratio was not explicitly used as a surrogate design

**Table 8. Measured or Calculated Values of Molar C/H Ratio, Net Heat of Combustion, and Smoke Point for the Target and Surrogate Fuels**

fuel type	molar C/H ratio	net heat of combustion <sup>a</sup> [MJ/kg]	smoke point <sup>b</sup> [mm]
CFA	0.561	42.90	13.4
CFA surrogate	0.550	43.15	13.7
FD9A	0.558	42.86	13.0
FD9A surrogate	0.539	43.05	14.4

<sup>a</sup>Measured per ASTM D 240.<sup>87</sup> <sup>b</sup>Measured per ASTM D 1322.<sup>88</sup>

property in this work, it is an important fuel parameter. The molar C/H ratios of the target fuels were calculated using

$$\frac{C}{H} = \frac{Y_C M_H}{Y_H M_C} \quad (10)$$

In eq 10,  $Y_C$  and  $Y_H$  are the mass fractions of carbon and hydrogen, respectively, in the fuels per ASTM D 5291 as provided in Table 1, and  $M_C$  and  $M_H$  are the atomic masses of carbon and hydrogen (12.011 g/mol and 1.008 g/mol, respectively). The molar C/H ratios of the surrogate fuels were calculated using

$$\frac{C}{H} = \frac{\sum_i X_i n_{C,i}}{\sum_i X_i n_{H,i}} \quad (11)$$

where  $X_i$  is the mole fraction of the  $i^{\text{th}}$  palette compound in the surrogate mixture;  $n_{C,i}$  and  $n_{H,i}$  are the number of moles of carbon and hydrogen per mole of palette-compound  $i$ , respectively; and the summation  $i$  runs over all palette compounds in the surrogate.

The more-pronounced *n*- and *iso*-alkane character of the surrogates evident in Figures 11 and 12 might lead one to expect significantly lower C/H ratios for the surrogates relative to their respective target fuels. While the C/H ratios of the CFA and FD9A surrogates are lower than those of the corresponding target fuels, the differences are small, at 1.9% and 3.4%, respectively. This good agreement is due to some of the cyclo-alkane, aromatic, and naphtho-aromatic palette compounds having higher C/H ratios than the target-fuel compounds that they were selected to represent, which attenuates the effect of the more-pronounced *n*- and *iso*-alkane character of the surrogates on the C/H ratios.

The net heat of combustion measurements for the target and surrogate fuels show excellent agreement: within 0.6% and 0.4%, respectively, for CFA and FD9A. In addition, the net heat of combustion of each surrogate fuel is equal to that of its corresponding target fuel within the 0.40 MJ/kg reproducibility of the ASTM D 240 test method.<sup>87</sup> The smoke-point measurements for the target and surrogate fuels also show excellent agreement, falling well within the 2-mm repeatability of the ASTM D 1322 test method.<sup>88</sup>

#### 4. SUMMARY AND CONCLUSIONS

The objective of this study was to develop a methodology to create a blend of ten or fewer pure compounds that adequately approximates the compositional, ignition-quality, and volatility characteristics of a real-world diesel fuel produced from refinery streams containing hundreds or thousands of compounds. Such simplified, “surrogate” diesel fuels are important for enabling computational engine optimization, for obtaining an improved

understanding of fuel effects on engine combustion and emissions processes, and for establishing time-invariant reference fuels for the diesel combustion-research community.

The methodology first employed  $^{13}\text{C}$  and  $^1\text{H}$  nuclear magnetic resonance (NMR) spectroscopy, the derived cetane number (DCN), and the advanced distillation curve (ADC) to quantify the compositional, ignition-quality, and volatility characteristics, respectively, of a real-world “target” diesel fuel. Next, a set of nine pure compounds (the “palette”) was selected to provide molecular structures and molecular weights representative of the major components of the target diesel fuel. Exact relationships and modeling assumptions relating the compositional, ignition-quality, and volatility characteristics of the individual palette compounds to their mixture properties were then coded into a regression model that automatically determined the composition of a mixture that would best match the same characteristics of the target fuel. The surrogate was then blended, and its known compositional characteristics and measured ignition-quality and volatility characteristics were compared to those of the target fuel. This process was completed for two target diesel fuels.

The primary results of the study are as follows:

1. Each eight-component surrogate diesel fuel created in this study contained all of the major hydrocarbon classes found in the target fuels, namely: *n*-alkanes; *iso*-alkanes; mono- and dicycloalkanes; mono- and diaromatics; and naphtho-aromatics.
2. Five of the eleven carbon-bond types determined by NMR analysis were matched for each target/surrogate-fuel pair to within the  $\pm 3$  mol % uncertainty of the measurement technique. The other six carbon-bond types showed differences averaging 7.3 mol %.
3. The DCN of each surrogate was, on average, higher than that of its respective target fuel by 1.7 DCN, a difference of 3.9%.
4. The ADC distillation temperature of each surrogate was, on average, 5.9 °C lower than that of its respective target fuel, a difference of 2.1%.
5. The density of each surrogate was 4.1% lower than that of its respective target fuel, on average.
6. Although they were not explicitly matched, other measured properties of the surrogates showed excellent agreement with their corresponding target-fuel values. The molar C/H ratios agreed to within 3.4%; the net heats of combustion agreed to within 0.6%; and the smoke points agreed to within the 2-mm repeatability of the test method.

Based on the above results, it is concluded that the methodology developed herein was successful at achieving the desired objectives of the study.

**Future Work.** Many of the challenges of matching the property targets discussed could be relieved somewhat by adding new palette compounds and reformulating the surrogates. In particular, it would be interesting to investigate the use of *iso*-alkane, aromatic, and cyclo-alkane compounds that are more representative of the constituents of these hydrocarbon classes in the target fuels. Efforts along these lines are currently underway. Single-cylinder metal- and/or optical-engine experiments with the surrogate and target fuels also are planned to assess the ability of the surrogate fuels to adequately mimic the mixing, combustion, and emissions characteristics of the target fuels. Further work also is warranted on determining

the identities, concentrations, formation mechanisms, and removal techniques for ignition-accelerating contaminants in the palette compounds. Although a number of research groups are using shock tubes, rapid compression machines, constant-volume vessels, and other facilities to measure ignition delays of palette compounds to assist in the development of chemical-kinetic models, the possibility of ignition-accelerating contaminants in the “pure” compounds used in these studies has not been discussed, and it is not clear that measures such as silica-gel treatment have been taken to remove these potential contaminants.

## ■ AUTHOR INFORMATION

### Corresponding Author

\*Phone: (925) 294-2223. Fax: (925) 294-1004. E-mail: cjmuell@sandia.gov.

### Notes

The authors declare no competing financial interest.

<sup>\$</sup>Deceased.

## ■ ACKNOWLEDGMENTS

This paper is dedicated to the memory of our friend and colleague Jim Franz. Funding for this research was provided by the U.S. Department of Energy (U.S. DOE) Office of Vehicle Technologies, and by the Coordinating Research Council (CRC) and the companies that employ the CRC members. The study was conducted under the auspices of CRC. The authors thank U.S. DOE program manager Kevin Stork for supporting the participation of the U.S. national laboratories in this study. C.J.M.’s portion of the research was conducted at the Combustion Research Facility, Sandia National Laboratories, Livermore, California. Sandia is a multiprogram laboratory operated by Sandia Corporation, a Lockheed Martin Company, for the U.S. DOE’s National Nuclear Security Administration under contract DE-AC04-94AL85000. W.J.P.’s portion of the research was performed under the auspices of the U.S. DOE at Lawrence Livermore National Laboratory under Contract DE-AC52-07NA27344. M.A.R.’s portion of the research was conducted at the National Renewable Energy Laboratory (NREL). The valuable technical assistance of NREL colleague Jon Luecke with surrogate treating, blending, and measurement of the ignition properties is gratefully acknowledged. NREL is operated by the Alliance for Sustainable Energy, LLC, for the U.S. DOE under contract DE-AC36-08GO28308. Rafal Gieleciak and Darcy Hager at the Natural Resources Canada (CanmetENERGY) Laboratory in Devon, Alberta, were responsible for the gas-chromatographic analyses of the fuels, palette compounds, and palette-compound mixtures, while Sara Salmon ran the proton and carbon NMR analyses. Elemental analyses were performed by the CanmetENERGY Analytical Group. The participation of CanmetENERGY in this project was funded by Natural Resources Canada through partial funding from the Canadian Program for Energy Research and Development and from the ecoEnergy Technology Initiative.

## ■ ABBREVIATIONS AND ACRONYMS

1MN = 1-methylnaphthalene (see Figure 9)

ADC = advanced distillation curve

ASTM = ASTM International (formerly American Society for Testing and Materials)

C = carbon

CFA = 2007 #2 ULSD Certification Fuel Batch A

CI = compression ignition  
 CN = cetane number  
 COV = coefficient of variation  
 CRC = Coordinating Research Council, Inc.  
 CT = carbon type  
 D86 = ASTM D 86 standard method and data  
 DCN = derived cetane number  
 DEPT = distortionless enhancement by polarization transfer  
 DOE = Department of Energy  
 EBP = end boiling point  
 FD9A = FACE Diesel No. 9 Batch A  
 FACE = fuels for advanced combustion engines  
 GC-FID = gas chromatography with flame ionization detection  
 GC-FIMS = gas chromatography with field ionization mass spectrometry  
 GC-SCD = gas chromatography with sulfur chemiluminescence detection  
 H = hydrogen  
 HMN = 2,2,4,6,8,8-heptamethylnonane (see Figure 9)  
 ID = ignition delay  
 IQT = ignition quality tester  
 MS = measured surrogate (a property value from a surrogate fuel)  
 MT = measured target (a property value from a target fuel)  
 NBCX = *n*-butylcyclohexane (see Figure 9)  
 NEI = *n*-eicosane (see Figure 9)  
 NHXD = *n*-hexadecane (see Figure 9)  
 NIST = National Institute of Standards and Technology  
 NMR = nuclear magnetic resonance spectroscopy  
 NOD = *n*-octadecane (see Figure 9)  
 PIONA = paraffins, *iso*-paraffins, olefins, naphthenes, and aromatics  
 PNLL = Pacific Northwest National Laboratory  
 PS = predicted surrogate (a property predicted for a surrogate fuel)  
 SGT = silica-gel treatment  
 TDEC = *trans*-decalin (see Figure 9)  
 TET = tetralin (see Figure 9)  
 TMB = 1,2,4-trimethylbenzene (see Figure 9)  
 ULSO = ultra-low-sulfur diesel  
 U.S. = United States

## ■ REFERENCES

- (1) De Ojeda, W.; Bulicz, T.; Han, X.; Zheng, M.; Cornforth, F. Impact of fuel properties on diesel low temperature combustion. *SAE Int. J. Engines* **2011**, *4* (1), 188–201, DOI: 10.4271/2011-01-0329.
- (2) Pickett, L. M.; Siebers, D. L. Non-sooting, low flame temperature mixing-controlled DI diesel combustion. *SAE Trans.* **2004**, *113* (4), 614–630, DOI: 10.4271/2004-01-1399.
- (3) Cheng, A. S.; Fisher, B. T.; Martin, G. C.; Mueller, C. J. Effects of fuel volatility on early direct-injection, low-temperature combustion in an optical diesel engine. *Energy Fuels* **2010**, *24* (3), 1538–1551.
- (4) Hildingsson, L.; Johansson, B.; Kalghatgi, G. T.; Harrison, A. J. Some effects of fuel autoignition quality and volatility in premixed compression ignition engines. *SAE Int. J. Engines* **2010**, *3* (1), 440–460, DOI: 10.4271/2010-01-0607.
- (5) Bessonette, P. W.; Schleyer, C. H.; Duffy, K. P.; Hardy, W. L.; Liechty, M. P. Effects of fuel property changes on heavy-duty HCCI combustion. *SAE Trans.* **2007**, *116* (3), 242–254, DOI: 10.4271/2007-01-0191.
- (6) Mueller, C. J.; Boehman, A. L.; Martin, G. C. An experimental investigation of the origin of increased NO<sub>x</sub> emissions when fueling a heavy-duty compression-ignition engine with soy biodiesel. *SAE Int. J. Fuels Lubr.* **2009**, *2* (1), 789–816, DOI: 10.4271/2009-01-1792.
- (7) Sjöberg, M.; Dec, J. E. Smoothing HCCI heat release with vaporization-cooling-induced thermal stratification using ethanol. *SAE Int. J. Fuels Lubr.* **2011**, *5* (1), 7–27, DOI: 10.4271/2011-01-1760.
- (8) Yang, Y.; Dec, J. E.; Dronniou, N.; Simmons, B. Characteristics of isopentanol as a fuel for HCCI engines. *SAE Int. J. Fuels Lubr.* **2010**, *3* (2), 725–741, DOI: 10.4271/2010-01-2164.
- (9) Polonowski, C. J.; Mueller, C. J.; Gehrke, C. R.; Bazyn, T.; Martin, G. C.; Lillo, P. M. An experimental investigation of low-soot and soot-free combustion strategies in a heavy-duty, single-cylinder, direct-injection, optical diesel engine. *SAE Int. J. Fuels Lubr.* **2011**, *5* (1), 51–77, DOI: 10.4271/2011-01-1812.
- (10) *Research Needs and Impacts in Predictive Simulation for Internal Combustion Engines (PreSICE)*; U.S. Dept. of Energy: Washington, DC, 2011.
- (11) *Basic Research for Clean and Efficient Combustion of 21st Century Transportation Fuels*; U.S. Dept. of Energy: Washington, DC, 2006.
- (12) Pitz, W. J.; Mueller, C. J. Recent progress in the development of diesel surrogate fuels. *Prog. Energy Combust. Sci.* **2011**, *37* (3), 330–350.
- (13) Pires da Cruz, A.; Dumas, J.-P.; Bruneaux, G. Two-dimensional in-cylinder soot volume fractions in diesel low temperature combustion mode. *SAE Int. J. Engines* **2011**, *4* (1), 2023–2047, DOI: 10.4271/2011-01-1390.
- (14) Brakora, J. L.; Ra, Y.; Reitz, R. D. Combustion model for biodiesel-fueled engine simulations using realistic chemistry and physical properties. *SAE Int. J. Engines* **2011**, *4* (1), 931–947, DOI: 10.4271/2011-01-0831.
- (15) Imren, A.; Golovitchev, V.; Sorusbay, C.; Valentino, G. The full cycle HD diesel engine simulations using KIVA-4 code. SAE Technical Paper 2010-01-2234, 2010.
- (16) Liang, L.; Naik, C. V.; Puduppakkam, K.; Wang, C.; Modak, A.; Meeks, E.; Ge, H.-W.; Reitz, R. D.; Rutland, C. Efficient simulation of diesel engine combustion using realistic chemical kinetics in CFD. SAE Technical Paper 2010-01-0178, 2010.
- (17) Honnet, S.; Seshadri, K.; Niemann, U.; Peters, N. A surrogate fuel for kerosene. *Proc. Combust. Inst.* **2009**, *32* (1), 485–492.
- (18) Lemaire, R.; Faccinetto, A.; Therssen, E.; Ziskind, M.; Focsa, C.; Desgroux, P. Experimental comparison of soot formation in turbulent flames of diesel and surrogate diesel fuels. *Proc. Combust. Inst.* **2009**, *32*, 737–744.
- (19) Ramirez, H. P.; Hadj-Ali, K.; Dievart, P.; Moreac, G.; Dagaut, P. Kinetics of oxidation of commercial and surrogate diesel fuels in a jet-stirred reactor: Experimental and modeling studies. *Energy Fuels* **2010**, *24*, 1668–1676.
- (20) Mathieu, O.; Djebaili-Chaumeix, N.; Paillard, C. E.; Douce, F. Experimental study of soot formation from a diesel fuel surrogate in a shock tube. *Combust. Flame* **2009**, *156* (8), 1576–1586.
- (21) Ra, Y.; Reitz, R. D. A vaporization model for discrete multi-component fuel sprays. *Int. J. Multiphase Flow* **2009**, *35* (2), 101–117.
- (22) Dooley, S.; Won, S. H.; Chaos, M.; Heyne, J.; Ju, Y. G.; Dryer, F. L.; Kumar, K.; Sung, C. J.; Wang, H. W.; Oehlschlaeger, M. A.; Santoro, R. J.; Litzinger, T. A. A jet fuel surrogate formulated by real fuel properties. *Combust. Flame* **2010**, *157* (12), 2333–2339.
- (23) Yang, Y.; Boehman, A. L.; Santoro, R. J. A study of jet fuel sootting tendency using the threshold soot index (TSI) model. *Combust. Flame* **2007**, *149* (1–2), 191–205.
- (24) Naik, C. V.; Puduppakkam, K.; Wang, C.; Kottalam, J.; Liang, L.; Hodgson, D.; Meeks, E. Applying detailed kinetics to realistic engine simulation: The surrogate blend optimizer and mechanism reduction strategies. *SAE Int. J. Engines* **2010**, *3* (1), 241–259, DOI: 10.4271/2010-01-0541.
- (25) Huber, M. L.; Lemmon, E. W.; Bruno, T. J. Surrogate mixture models for the thermophysical properties of aviation fuel Jet-A. *Energy Fuels* **2010**, *24*, 3565–3571.
- (26) Alnajjar, M.; Cannella, W.; Dettman, H.; Fairbridge, C.; Franz, J.; Gallant, T.; Gieleciak, R.; Hager, D.; Lay, C.; Lewis, S.; Ratcliff, M.; Sluder, S.; Storey, J.; Yin, H.; Zigler, B. *Chemical and Physical Properties of the Fuels for Advanced Combustion Engines (FACE) Research Diesel Fuels*, FACE-1; Coordinating Research Council: Alpharetta, GA, 2010.

- (27) Diesel 2007 ULSD (7–15 ppm) Certification Fuel, Chevron Phillips Chemical Company, Sept. 24, 2008. Available online: [http://www.cpchem.com/enu/tds\\_unsecured/Diesel\\_2007\\_ULSD.pdf](http://www.cpchem.com/enu/tds_unsecured/Diesel_2007_ULSD.pdf) (Accessed: Mar. 31, 2010).
- (28) *Standard Test Method for Determination of the Aromatic Content and Polynuclear Aromatic Content of Diesel Fuels and Aviation Turbine Fuels by Supercritical Fluid Chromatography*, ASTM Standard D 5186-03; ASTM International: West Conshohocken, PA, 2003.
- (29) *Standard Test Method for Hydrocarbon Types in Liquid Petroleum Products by Fluorescent Indicator Absorption*, ASTM Standard D 1319; ASTM International: West Conshohocken, PA, 2010.
- (30) *Standard Test Method for Hydrocarbon Types in Middle Distillates by Mass Spectrometry*, ASTM Standard D 2425; ASTM International: West Conshohocken, PA, 2004.
- (31) *Standard Test Method for Bromine Numbers of Petroleum Distillates and Commercial Aliphatic Olefins by Electrometric Titration*, ASTM Standard D 1159; ASTM International: West Conshohocken, PA, 2007.
- (32) Farrell, J. T.; Cernansky, N. P.; Dryer, F. L.; Friend, D. G.; Hergart, C. A.; Law, C. K.; McDavid, R. M.; Mueller, C. J.; Patel, A. K.; Pitsch, H. Development of an experimental database and kinetic models for surrogate diesel fuels. SAE Technical Paper 2007-01-0201, 2007.
- (33) Japanwala, S.; Chung, K. H.; Dettman, H. D.; Gray, M. R. Quality of distillates from repeated recycle of residue. *Energy Fuels* **2002**, *16* (2), 477–484.
- (34) *Standard Test Method for Cetane Number of Diesel Fuel Oil*, ASTM Standard D 613; ASTM International: West Conshohocken, PA, 2008.
- (35) *Standard Test Method for Determination of Ignition Delay and Derived Cetane Number (DCN) of Diesel Fuel Oils by Combustion in a Constant Volume Chamber*, ASTM Standard D 6890-10a; ASTM International: West Conshohocken, PA, 2010.
- (36) Kister, H. Z. *Distillation Operation*; McGraw-Hill: New York, 1988.
- (37) Kister, H. Z. *Distillation Design*; McGraw-Hill: New York, 1991.
- (38) Leffler, W. L. *Petroleum Refining in Nontechnical Language*; PennWell: Tulsa, OK, 2000.
- (39) Fair, J. R. Distillation. In *Kirk Othmer Encyclopedia of Chemical Technology*; Wiley Interscience, John Wiley and Sons, Inc.: New York, 2004; Vol. 8, pp 739–785.
- (40) *Standard Test Method for Distillation of Petroleum Products at Atmospheric Pressure*, ASTM Standard D 86-04b; ASTM International: West Conshohocken, PA, 2004.
- (41) Bruno, T. J.; Ott, L. S.; Smith, B. L.; Lovestead, T. M. Complex fluid analysis with the advanced distillation curve approach. *Anal. Chem.* **2010**, *82*, 777–783.
- (42) Bruno, T. J.; Ott, L. S.; Lovestead, T. M.; Huber, M. L. The composition explicit distillation curve technique: relating chemical analysis and physical properties of complex fluids. *J. Chromatogr.* **2010**, *A1217*, 2703–2715.
- (43) Bruno, T. J.; Ott, L. S.; Lovestead, T. M.; Huber, M. L. Relating complex fluid composition and thermophysical properties with the advanced distillation curve approach. *Chem. Eng. Technol.* **2010**, *33* (3), 363–376.
- (44) Bruno, T. J. Improvements in the measurement of distillation curves. 1. A composition-explicit approach. *Ind. Eng. Chem. Res.* **2006**, *45* (12), 4371–4380.
- (45) Bruno, T. J.; Smith, B. L. Improvements in the measurement of distillation curves. 2. Application to aerospace/aviation fuels RP-1 and S-8. *Ind. Eng. Chem. Res.* **2006**, *45* (12), 4381–4388.
- (46) Bruno, T. J. Method and apparatus for precision in-line sampling of distillate. *Sep. Sci. Technol.* **2006**, *41* (2), 309–314.
- (47) Huber, M. L.; Smith, B. L.; Ott, L. S.; Bruno, T. J. Surrogate mixture model for the thermophysical properties of synthetic aviation fuel S-8: Explicit application of the advanced distillation curve. *Energy Fuels* **2008**, *22*, 1104–1114.
- (48) Huber, M. L.; Lemmon, E. W.; Diky, V.; Smith, B. L.; Bruno, T. J. Chemically authentic surrogate mixture model for the thermophysical properties of a coal-derived-liquid fuel. *Energy Fuels* **2008**, *22*, 3249–3257.
- (49) Huber, M. L.; Lemmon, E. W.; Ott, L. S.; Bruno, T. J. Preliminary surrogate mixture models for rocket propellants RP-1 and RP-2. *Energy Fuels* **2009**, *23*, 3083–3088.
- (50) Bruno, T. J.; Smith, B. L. Enthalpy of combustion of fuels as a function of distillate cut: Application of an advanced distillation curve method. *Energy Fuels* **2006**, *20*, 2109–2116.
- (51) Ott, L. S.; Hadler, A.; Bruno, T. J. Variability of the rocket propellants RP-1, RP-2, and TS-5: Application of a composition- and enthalpy-explicit distillation curve method. *Ind. Eng. Chem. Res.* **2008**, *47* (23), 9225–9233.
- (52) Bruno, T. J.; Wolk, A.; Naydich, A. Stabilization of biodiesel fuel at elevated temperature with hydrogen donors: Evaluation with the advanced distillation curve method. *Energy Fuels* **2009**, *23*, 1015–1023.
- (53) Bruno, T. J.; Baibourine, E. Analysis of organometallic gasoline additives with the composition-explicit distillation curve method. *Energy Fuels* **2010**, *24*, 5508–5513.
- (54) Ott, L. S.; Smith, B. L.; Bruno, T. J. Advanced distillation curve measurements for corrosive fluids: application to two crude oils. *Fuel* **2008**, *87*, 3055–3064.
- (55) Bruno, T. J.; Smith, B. L. Evaluation of the physicochemical authenticity of aviation kerosene surrogate mixtures Part I: Analysis of volatility with the advanced distillation curve. *Energy Fuels* **2010**, *24*, 4266–4276.
- (56) Bruno, T. J.; Huber, M. L. Evaluation of the physicochemical authenticity of aviation kerosene surrogate mixtures Part II: Analysis and prediction of thermophysical properties. *Energy Fuels* **2010**, *24*, 4277–4284.
- (57) Smith, B. L.; Bruno, T. J. Advanced distillation curve measurement with a model predictive temperature controller. *Int. J. Thermophys.* **2006**, *27*, 1419–1434.
- (58) Ott, L. S.; Smith, B. L.; Bruno, T. J. Experimental test of the Sydney Young equation for the presentation of distillation curves. *J. Chem. Thermodynam.* **2008**, *40*, 1352–1357.
- (59) Young, S. Correction of boiling points of liquids from observed to normal pressures. *Proc. Chem. Soc.* **1902**, *81*, 777.
- (60) Bruno, T. J.; Lovestead, T. M.; Riggs, J. R.; Jorgenson, E. L.; Huber, M. L. Comparison of diesel fuel oxygenate additives with the composition-explicit distillation curve method. Part 1: Linear compounds with one to three oxygens. *Energy Fuels* **2011**, *25* (6), 2493–2507.
- (61) Bruno, T. J.; Lovestead, T. M.; Huber, M. L.; Riggs, J. R. Comparison of diesel fuel oxygenate additives with the composition-explicit distillation curve method. Part 2: Cyclic compounds with one to two oxygens. *Energy Fuels* **2011**, *25* (6), 2508–2517.
- (62) Lovestead, T. M.; Bruno, T. J. Comparison of diesel fuel oxygenate additives with the composition-explicit distillation curve method. Part 3: t-butyl glycerols. *Energy Fuels* **2011**, *25* (6), 2518–2525.
- (63) Smith, B. L.; Ott, L. S.; Bruno, T. J. Composition-explicit distillation curves of diesel fuel with glycol ether and glycol ester oxygenates: A design tool for decreased particulate emissions. *Environ. Sci. Technol.* **2008**, *42* (20), 7682–7689.
- (64) Taylor, B. M.; Kuyatt, C. E. *Guidelines for Evaluating and Expressing Uncertainty of NIST Measurement Results*, NIST Technical Note 1297; U.S. Government Printing Office: Washington, DC, 1994.
- (65) *Standard Test Method for Density, Relative Density, and API Gravity of Liquids by Digital Density Meter*, ASTM Standard D 4052; ASTM International: West Conshohocken, PA, 2009.
- (66) Lemmon, E. W.; McLinden, M. O.; Huber, M. L. *REFPROP, Reference Fluid Thermodynamic and Transport Properties, NIST Standard Reference Database 23, V9*; National Institute of Standards and Technology: Gaithersburg, MD, 2010.
- (67) Gmehling, J.; Menke, J.; Krafczk, J.; Fischer, K. *Azeotropic Data, Parts 1, 2, and 3*; Wiley VCH: Weinheim, 2004.
- (68) Bruno, T. J.; Huber, M. L.; Laesecke, A.; Lemmon, E. W.; Perkins, R. A. *Thermochemical and Thermophysical Properties of JP-10*,

- NIST-IR 6640; National Institute of Standards and Technology: Boulder, CO, 2006.
- (69) Hadler, A. B.; Ott, L. S.; Bruno, T. J. Study of azeotropic mixtures with the advanced distillation curve approach. *Fluid Phase Equilib.* **2009**, *281* (1), 49–59.
- (70) Westbrook, C. K.; Pitz, W. J.; Herbinet, O.; Curran, H. J.; Silke, E. J. A comprehensive detailed chemical kinetic reaction mechanism for combustion of *n*-alkane hydrocarbons from *n*-octane to *n*-hexadecane. *Combust. Flame* **2009**, *156* (1), 181–199.
- (71) Murphy, M. J.; Taylor, J. D.; McCormick, R. L. *Compendium of Experimental Cetane Number Data*, NREL Report No. SR-540-36805; National Renewable Energy Laboratory: Golden, CO, 2004.
- (72) Westbrook, C. K.; Pitz, W. J.; Mehl, M.; Curran, H. J. Detailed chemical kinetic reaction mechanisms for primary reference fuels for diesel cetane number and spark-ignition octane number. *Proc. Combust. Inst.* **2011**, *33*, 185–192.
- (73) Oehlschlaeger, M. A.; Steinberg, J.; Westbrook, C. K.; Pitz, W. J. The autoignition of iso-cetane at high to moderate temperatures and elevated pressures: Shock tube experiments and kinetic modeling. *Combust. Flame* **2009**, *156* (11), 2165–2172.
- (74) Wang, H.; Warner, S. J.; Oehlschlaeger, M. A.; Bounaceur, R.; Biet, J.; Glaude, P. A.; Battin-Leclerc, F. An experimental and kinetic modeling study of the autoignition of  $\alpha$ -methylnaphthalene/air and  $\alpha$ -methylnaphthalene/*n*-decane/air mixtures at elevated pressures. *Combust. Flame* **2010**, *157* (10), 1976–1988.
- (75) Pitsch, H. Detailed kinetic reaction mechanism for ignition and oxidation of  $\alpha$ -methylnaphthalene. *26th Symp. (Int.) Combustion* **1996**, 721–728.
- (76) Bounaceur, R.; Glaude, P. A.; Fournet, R.; Battin-Leclerc, F.; Jay, S.; da Cruz, A. P. Kinetic modelling of a surrogate diesel fuel applied to 3D auto-ignition in HCCI engines. *Int. J. Vehicle Des.* **2007**, *44* (1–2), 124–142.
- (77) Linstrom, P. J.; Mallard, W. G. *NIST Chemistry WebBook*, NIST Standard Reference Database No. 69; National Institute of Standards and Technology: Gaithersburg, MD, 2005. Available online: <http://webbook.nist.gov>.
- (78) Gieleciak, R.; Hager, D. *Estimation of Purity of Compounds for Diesel Fuel Surrogate Blends*, Division Report Devon 10-68 (CF); CanmetENERGY: Devon, Alberta, Canada, 2010.
- (79) Doddrell, D. M.; Pegg, D. T.; Bendall, M. R. Distortionless enhancement of NMR signals by polarization transfer. *J. Magn. Reson.* **1982**, *48* (2), 323–327.
- (80) Sarathy, S. M.; Westbrook, C. K.; Mehl, M.; Pitz, W. J.; Togbé, C.; Dagaut, P.; Wang, H.; Oehlschlaeger, M. A.; Niemann, U.; Seshadri, K.; Veloo, P. S.; Ji, C.; Egolfopoulos, F. N.; Lu, T. Comprehensive chemical kinetic modeling of the oxidation of 2-methylalkanes from C7 to C20. *Combust. Flame* **2011**, *158*, 2338–2357.
- (81) Heyne, J. S.; Boehman, A. L.; Kirby, S. Autoignition studies of *trans*- and *cis*-decalin in an ignition quality tester (IQT) and the development of a high thermal stability unifuel/single battlefield fuel. *Energy Fuels* **2009**, *23*, 5879–5885.
- (82) Fairbridge, C. Personal communication to W. J. Cannella, Oct. 21, 2009.
- (83) Hochhauser, A. M. *Review of Prior Studies of Fuel Effects on Vehicle Emissions*, CRC Report No. E-84; Coordinating Research Council: Alpharetta, GA, 2008.
- (84) Wallace, L. A.; Renz, M. C. *Use of Column Chromatography to Improve the Ignition Delay Characteristics of Impure Methylcyclohexane in the ASTM D 7170 FIT Combustion Analyzer*, Report to ASTM Subcommittee D02.01; Dixie Services Inc.: Galena Park, TX, 2008.
- (85) Bizub, J. J. Personal communication to C. J. Mueller, June 9, 2011.
- (86) Bizub, J. J. *MCH Contamination Effects. D7170 ID Results*, Report to ASTM Subcommittee D02.01, Section E; Kansas City, Missouri, 2010.
- (87) *Heat of Combustion of Liquid Hydrocarbon Fuels by Bomb Calorimeter*, ASTM Standard D 240-09; ASTM International: West Conshohocken, PA, 2009.
- (88) *Standard Test Method for Smoke Point of Kerosine and Aviation Turbine Fuel*, ASTM Standard D 1322-08; ASTM International: West Conshohocken, PA, 2008.